

**Advanced novel imaging tools
for detection of early morphological and
functional impairment
in cardiovascular diseases**

PhD thesis

Maria Lembo, MD



UNIVERSITÀ DEGLI STUDI DI NAPOLI
FEDERICO II



THE UNIVERSITY
of EDINBURGH

Advanced novel imaging tools for detection of early morphological and functional impairment in cardiovascular diseases

PhD thesis

Maria Lembo, MD

22/06/1988 Naples (Italy)

Promoters: Prof. Maurizio Galderisi[†], Prof. Raffaele Izzo

*Department of Advanced Biomedical Sciences,
Federico II University of Naples, Italy*

Co-promotor: Prof. Marc Dweck

*British Heart Foundation Centre of Cardiovascular Science,
University of Edinburgh, UK*

Naples,

Federico II University of Naples, Faculty of Medicine,

Via Pansini n. 5, 80131 Naples, Italy

*“Do not go where the path may lead,
go instead where there is no path and leave a trail.”*

Ralph Waldo Emerson

Contents

Chapter 1.	General introduction and outline of the thesis	pag. 6
-------------------	--	--------

Part I. Advanced cardiac ultrasound imaging for identification of early impairment in Hypertensive Heart Disease

Chapter 2.	Advanced imaging tools for evaluating cardiac morphological and functional impairment in hypertensive disease. <i>Published in J Hypertens. 2021. doi:10.1097/HJH.0000000000002967. Online ahead of print.</i>	pag. 12
-------------------	---	---------

Chapter 3.	Three-dimensional echocardiographic ventricular mass/end-diastolic volume ratio in native hypertensive patients: relation between stroke volume and geometry. <i>Published in J Hypertens. 2018 Aug;36(8):1697-1704.</i>	pag. 16
-------------------	---	---------

Chapter 4.	Impact of left ventricular mass/end-diastolic volume ratio by three-dimensional echocardiography on two-dimensional global longitudinal strain and diastolic function in native hypertensive patients. <i>Published in J Hypertens. 2019 Oct;37(10):2041-2047.</i>	pag. 20
-------------------	---	---------

Chapter 5.	Interrelation between midwall mechanics and longitudinal strain in newly diagnosed and never-treated hypertensive patients without clinically defined hypertrophy. <i>Published in J Hypertens. 2020 Feb;38(2):295-302.</i>	pag. 24
-------------------	--	---------

- Chapter 6.** Prominent basal and middle strain longitudinal involvement in newly-diagnosed and never treated hypertensive patients without clear-cut hypertrophy. pag. 28
Published in Int J Cardiol. 2020 Apr 1;304:179-184.
- Chapter 7.** Identification of cardiac organ damage in arterial hypertension: insights by echocardiography for a comprehensive assessment. pag. 31
Published in J Hypertens. 2020 Apr;38(4):588-598.
- Chapter 8.** Mechano-energetic efficiency as a predictor of left ventricular systolic dysfunction in hypertensive patients with optimal blood pressure control: the Campania Salute Network. pag. 34
Under peer review.

Part II. Advanced ultrasound cardiac imaging in other cardiovascular diseases

- Chapter 9.** Strain-oriented strategy for guiding cardioprotection initiation of breast cancer patients experiencing cardiac dysfunction. pag. 37
Published in Eur Heart J Cardiovasc Imaging. 2019 Dec 1;20(12):1345-1352.
- Chapter 10.** Prominent longitudinal strain reduction of left ventricular basal segments in treatment-naïve Anderson-Fabry disease patients. pag. 41
Published in Eur Heart J Cardiovasc Imaging. 2019 Apr 1;20(4):438-445.
- Chapter 11.** Left ventricular diastolic abnormalities other than valvular heart disease in antiphospholipid syndrome: An echocardiographic study. pag. 45
Published in Int J Cardiol. 2018 Nov 15;271:366-370.

Chapter 12.	Cardiac Manifestations of Antiphospholipid Syndrome: Clinical Presentation, Role of Cardiac Imaging, and Treatment Strategies. <i>Published in Semin Thromb Hemost. 2019 Jul;45(5):468-477.</i>	pag. 47
Chapter 13.	Impaired Right and Left Ventricular Longitudinal Function in Patients with Fibrotic Interstitial Lung Diseases. <i>Published in J Clin Med. 2020 Feb 21;9(2):587.</i>	pag. 50
Chapter 14.	Cardiopulmonary exercise testing and echocardiographic exam: a useful interaction. <i>Published in Cardiovasc Ultrasound. 2019 Dec 3;17(1):29.</i>	pag. 53
Chapter 15.	Global longitudinal strain is a hallmark of cardiac damage in mitral regurgitation: the Italian arm of the European Registry of mitral regurgitation. <i>Published in Cardiovasc Ultrasound. 2019 Nov 21;17(1):28. doi: 10.1186/s12947-019-0178-7.</i>	pag. 55
Chapter 16.	Practical Impact of New Diastolic Recommendations on Noninvasive Estimation of Left Ventricular Diastolic Function and Filling Pressures. <i>Published in J Am Soc Echocardiogr. 2020 Feb;33(2):171-181.</i>	pag. 57

Part III. Advanced imaging tools for evaluation of fibrocalcific score in aortic valve stenosis: the use of contrast-CT

- Chapter 17.** Contrast-enhanced computed tomography assessment of aortic stenosis. pag. 60
Published in Heart. 2021 Jan 29:heartjnl-2020-318556. doi: 10.1136/heartjnl-2020-318556. Online ahead of print.
- Chapter 18.** Gaussian mixture model for evaluation of fibrocalcific score in aortic valve stenosis. pag. 64
Under peer review.

Part IV. Advanced molecular imaging of thoracic aorta by 18F-Sodium Fluoride PET-CT for identification of microcalcification activity and stroke risk prediction

- Chapter 19.** Quantifying microcalcification activity in the thoracic aorta. pag. 69
Published in J Nucl Cardiol. 2021 Jan 20. doi: 10.1007/s12350-020-02458-w. Online ahead of print.
- Chapter 20.** Thoracic Aortic 18F-Sodium Fluoride Activity and the Risk of Ischaemic Stroke in Patients with Established Cardiovascular Disease. *Under peer review.* pag. 72

Part V. Discussion and conclusions

Discussion	pag. 77
Conclusions	pag. 86
List of abbreviations	pag. 87
Bibliography	pag. 89
Curriculum vitae	pag. 98
Acknowledgments	pag. 116

CHAPTER 1

General introduction and outline of the thesis

Advanced imaging tools provide detailed information about the structure and function of the heart and the cardiovascular system, essential in both the diagnostic process and patients' management. Early diagnosis of cardiac modifications and arterial disease together with the identification of subclinical organ damage has become crucial for a timely and adequate treatment, aiming at not only the avoidance of irreparable organ damage but also trying to confine injury progression ¹.

Beyond standard echo-Doppler echocardiography, which remains among the most simple but accurate methods for the investigation of cardiac and vascular remodelling and systolic and diastolic dysfunction, advanced imaging techniques are emerging for their sensitive capability of recognizing early myocardial and vascular impairment in many cardiovascular diseases ^{1,2}. Those imaging methods, including speckle tracking and three-dimensional (3D) echocardiography, cardiac magnetic resonance imaging (MRI), computed tomography (CT) and Positron emission tomography-computed tomography (PET-CT), can help, in different ways, in the detection of subclinical disease and/or in the identification of cardiovascular changes.

Those techniques are able to ameliorate diagnostic accuracy and provide markers to further improve risk prediction and optimize patient care. In addition, imaging tools are easily applicable into both clinical and research practice thanks to novel approaches and software advancements which sensibly reduce the time for analyses.

Outline of the thesis

The thesis is structured in five parts:

Part I. Advanced cardiac ultrasound imaging for identification of early impairment in Hypertensive Heart Disease

In the first section of the thesis we report our papers published in the field of advanced cardiac imaging in hypertensive heart disease. We put emphasis on the use of advanced echocardiographic techniques such as speckle tracking echo and 3D echocardiography for the identification of early morphological and functional impairment in the hypertensive setting. Speckle tracking echocardiography, a simple and feasible ultrasound technique that can be easily performed during a standard echocardiographic exam, provides a quantitative analysis of left ventricular (LV) deformation in the three orthogonal planes (longitudinal, circumferential and radial) and left ventricular twisting ³⁻⁵. Among the different LV deformation components, global longitudinal strain (GLS) has been identified to be an earlier marker of subclinical cardiac impairment than left ventricular ejection fraction (LVEF) ⁶⁻⁸. It is also associated with both the degree of LV filling pressures and the extent of myocardial fibrosis in uncomplicated hypertensive patients ⁹. We evaluated regional LV patterns of longitudinal strain and base-to-apex behavior in newly diagnosed, never-treated hypertensive patients without LV hypertrophy. We also investigated longitudinal (by GLS) and circumferential (by midwall fractional shortening, MFS) systolic function and correlations between these two functional components in early stages of arterial hypertension.

On the other hand, 3D-echocardiography allows computation of LV volumes and LVM with an accuracy comparable with cardiac MRI ¹⁰⁻¹². We evaluated

the ability of 3D- echocardiography in identifying a phenotype of LV concentric geometry according to LV mass/ end-diastolic volume ratio, possibly detecting early myocardial morphological and functional (both systolic by LV stroke volume and GLS and diastolic function) damage in native-hypertensive patients. Furthermore, we also explored possible echo parameters as predictors of future systolic dysfunction in patients affected by arterial hypertension.

Part II. Advanced ultrasound cardiac imaging in other cardiovascular diseases.

In the second part of the thesis, we report a cluster of papers focusing on the role of ultrasound imaging tools for the identification of early cardiac impairment in several cardiovascular diseases. In particular we analyzed the advantage of using GLS approach for identification of subclinical cancer therapy related LV dysfunction and a strain guided strategy for initiation of cardioprotective drugs in patients experiencing cardiotoxicity and affected by breast cancer, undergoing potentially harmful chemotherapy. In addition, we evaluated the role of advanced echocardiography for detection of early LV dysfunction in Anderson-Fabry disease, antiphospholipid syndrome and mitral regurgitation, all conditions in which cardiac involvement can occur. Furthermore, we investigated right ventricular function by both right ventricular longitudinal strain and 3D- echocardiography in patients affected by fibrotic interstitial lung disease.

Part III. Advanced imaging tools for evaluation of fibrocalcific score in aortic valve stenosis: the use of contrast-CT.

In this section of the thesis we focus on the role of contrast computed tomography for evaluation of the fibrocalcific volume in aortic valve stenosis. Guidelines recommend non-contrast CT calcium scoring of the aortic valve (CT-AVC) as an arbiter of aortic stenosis severity when echocardiographic measurements are discordant¹³, on the basis of data demonstrating the diagnostic accuracy of CT-AVC as a flow-independent measure and its correlation with disease progression and clinical events ¹⁴⁻¹⁶. However, CT-AVC has several important limitations: it offers little detail about valve morphology and is unable to localise the anatomical distribution of calcium in the valve and surrounding structures. In addition, CT-AVC cannot quantify fibrosis, an important contributor to valve stenosis, and may therefore misclassify disease severity, particularly in young females and those with bicuspid valves ^{17, 18}. On the other hand, contrast CT angiography is widely used to assess and quantify calcific and non-calcific plaques in the coronary vasculature ¹⁹. It is the gold standard method of anatomical assessment before transcatheter aortic valve intervention and is routinely incorporated into clinical workflows ^{20, 21}. Thus, we investigated the use of contrast-enhanced cardiac CT to evaluate aortic valve calcium volumes and also non-calcific leaflet thickening as a marker of valve fibrosis, using also novel approaches as the computation of volumes according to a gaussian mixture model calibrated against blood pool radiodensity, reducing drastically the time for analysis.

Part IV. Advanced molecular imaging of thoracic aorta by 18F-Sodium Fluoride PET-CT for identification of microcalcification activity and stroke risk prediction.

18F-Sodium fluoride (18F-NaF) is a positron emitting radiotracer that allows the detection of microcalcification activity by positron emission tomography

(PET),²² providing a marker of aortic disease which might further improve risk prediction. Indeed, coronary ¹⁸F-NaF PET has recently demonstrated its ability to improve risk prediction beyond the one afforded by CT calcium score ^{23, 24}. Thus, there is interest in developing summary quantitative methods of measuring ¹⁸F-NaF uptake in the aorta, which may provide similarly important prognostic information. Quantification of ¹⁸F-sodium fluoride uptake in the thoracic aorta currently involves labour intensive analysis of multiple regions of interest across sequential axial slices and calculating mean and maximum intensity uptake values. These values are then normalized to blood pool activity to generate mean (TBRmean) and maximum (TBRmax) tissue to background ratios respectively ^{25, 26}. Typically, TBRmax values are influenced by only a small number of the most intense pixels within a volume of interest and may not accurately reflect the overall PET activity within that volume. A simple, robust and time-efficient technique that could provide a summary measure of PET uptake across the thoracic aorta would be a major advance. We, therefore, aimed to develop a novel method of quantifying the burden of ¹⁸F-NaF uptake across both the ascending aorta and aortic arch (aortic microcalcification activity, AMA) and to assess its repeatability, reproducibility and time-efficiency compared with current standard approaches. We also applied this assessment in a setting of patients with established cardiovascular disease in order to study AMA as a possible predictor of ischemic stroke.

Part V: Discussion and conclusions. The last section of the thesis is a discussion of the results obtained according to the several addressed topics with the conclusions.

Part I

Advanced cardiac ultrasound imaging
for identification of early impairment
in Hypertensive Heart Disease

CHAPTER 2

Advanced imaging tools for evaluating cardiac morphological and functional impairment in hypertensive disease

Advanced imaging techniques, such as speckle tracking and 3D echocardiography, cardiac MRI, CT and PET-CT, are able to identify cardiovascular injury at different stages of arterial hypertension, from subclinical alterations and overt organ damage to possible complications related to pressure overload ²⁷⁻²⁹, thus giving a precious contribution for guiding timely and appropriate management of patients and therapy, in order to improve diagnostic accuracy and prevent disease progression.

The present review focuses on the peculiarity of different advanced imaging tools to provide information about different and multiple morphological and functional aspects involved in the hypertensive cardiovascular injury. This evaluation emphasizes the usefulness of the emerging multi-imaging approach for a comprehensive overview of arterial hypertension induced cardiovascular damage.

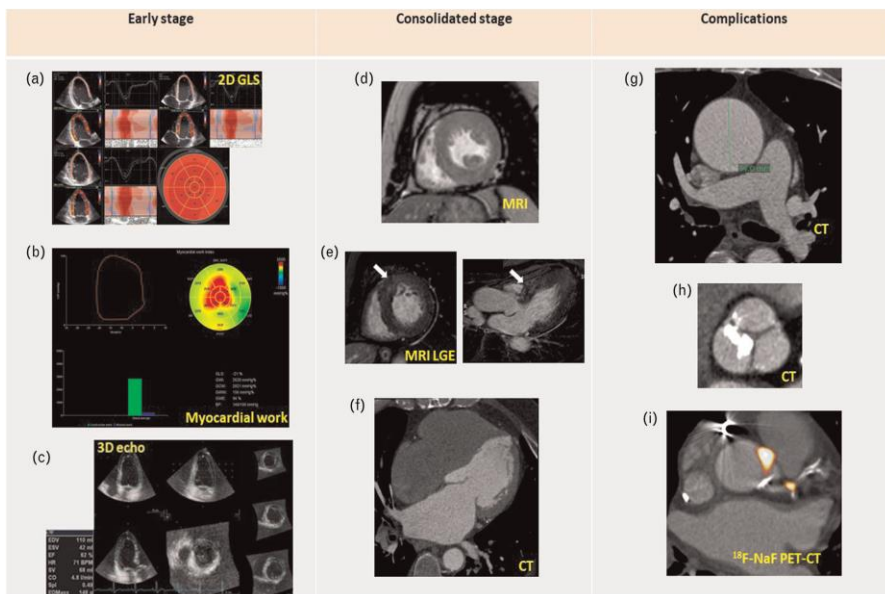


Figure 1. Example showing alterations provided by different advanced imaging tools at early stage, consolidated stage of arterial hypertension and complications. At early stages: (a) 2D GLS and regional strain impairment with predominant involvement of basal and middle longitudinal strain, (b) Myocardial work components alteration in hypertensive patients, (c) LV concentric geometry with increased LVM/EDV ratio detectable at 3D-echocardiography. At consolidated stage: (d) LVH evaluated by MRI, (e) LGE nonischemic intramyocardial pattern (white arrow) of the basal anterior septum (left: basal short axis view, right: three-chamber view) in a hypertensive patient with LVH, (f) contrast-enhanced CT showing LA dilation. Complications: (g) Aneurism of the ascending aorta detected by contrast-CT, (h) Aortic valve calcification and stenosis by CT, (i) 18F-NaF PET-CT showing uptake within both the descending left coronary artery and the aortic valve. 18F-NaF, fluorine-18-sodium fluoride; 2D, two-dimensional; 3D, three-dimensional; CT, computed tomography; EDV, end-diastolic volume; GLS, global longitudinal strain; LA, left atrial; LV, left ventricular; LVH, left ventricular hypertrophy; LVM, left ventricular mass; PET-CT, PET-computed tomography.

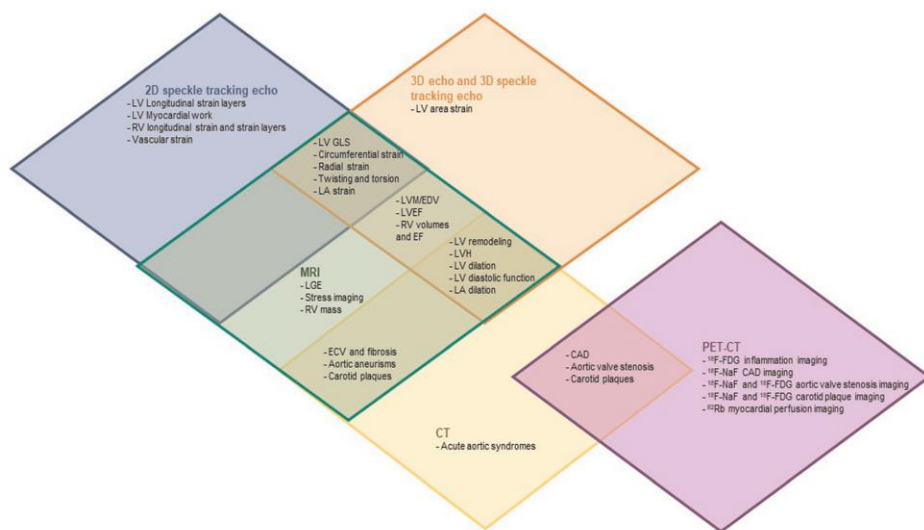


Figure 2. Schema depicting the advanced imaging tools useful in the cardiac and vascular damage induced by arterial hypertension; some evaluations are common to one or more techniques while each method owns its peculiarities. 18F-FDG, fluorine-18-fluorodeoxyglycose; 18F-NaF, fluorine-18-sodium fluoride; 2D, two-dimensional; 3D, three-dimensional; CAD, coronary artery disease; CT, computed tomography; ECV, extracellular volume fraction; EDV, end-diastolic volume; GLS, global longitudinal strain; LA, left atrial; LGE, late gadolinium enhancement; LV, left ventricular; LVH, left ventricular hypertrophy; LVM, left ventricular mass; PET-CT, PET-computed tomography.

The great advancements in imaging techniques allow the evaluation of arterial hypertension condition and influence on the myocardium and the cardiovascular system from multiple points of view, from tools bringing to light subclinical dysfunction as speckle tracking echocardiography, to instruments allowing evaluation of tissue characterization and possible arterial hypertension complication as MRI and CT, and molecular imaging highlighting active metabolism, calcification activity or microvascular

dysfunction. Different imaging tools are able to detect morphological and functional abnormalities related to arterial hypertension, but, on the contrary, every single technique owns its peculiarity and provides complementary information (Figure. 2). A multi-imaging approach thus may help to have a more exhaustive perspective of hypertensive-induced damage, thus contributing to assess an early diagnosis, avoid disease progression and provide appropriate treatments for patients' optimal management.

CHAPTER 3

Three-dimensional echocardiographic ventricular mass/end-diastolic volume ratio in native hypertensive patients: relation between stroke volume and geometry.

Background: Elevated left ventricular (LV) mass/end diastolic volume ratio (LVM/EDV) ratio by cardiac MRI is associated with higher myocardial fibrosis and dysfunction and even with adverse prognosis in the hypertensive setting ^{28, 30}. However, cardiac MRI has high costs and limited availability. Real-time 3D echocardiography, allows calculation of LV volumes and mass (LVM) with an accuracy comparable with cardiac MRI ¹⁰⁻¹². Accordingly, we designed this study to investigate whether a 3D echocardiographic approach could show similar ability of MRI in detecting LV geometry patterns by using LVM/ EDV ratio and identify possible 3D-echocardiographic parameters, as LV stroke volume, which could detect early pump dysfunction in native hypertensive patients. As antihypertensive therapy might positively alter and delay cardiac progressive remodeling and consequences on LV pump performance ^{31, 32}, we studied a population of newly diagnosed, never-treated hypertensive patients.

Methods: One hundred and twenty-eight native hypertensive patients underwent two dimensional (2D) and 3D echocardiography. 3D assessment was performed according to a previously described methodology ³³, which included automatic slicing of full LV volume data set, alignment by pivoting and translating the four-chamber plane, automated identification of endocardia border both at end-diastole and end-systole.

The population was divided into two groups, according to cut-off point values of 3D-LVM/EDV ratio corresponding to its upper 95% confidence interval in a population of 90 healthy normotensive individuals: LVM/EDV ratio cut-off was 1.22 in men and 1.23 in women.

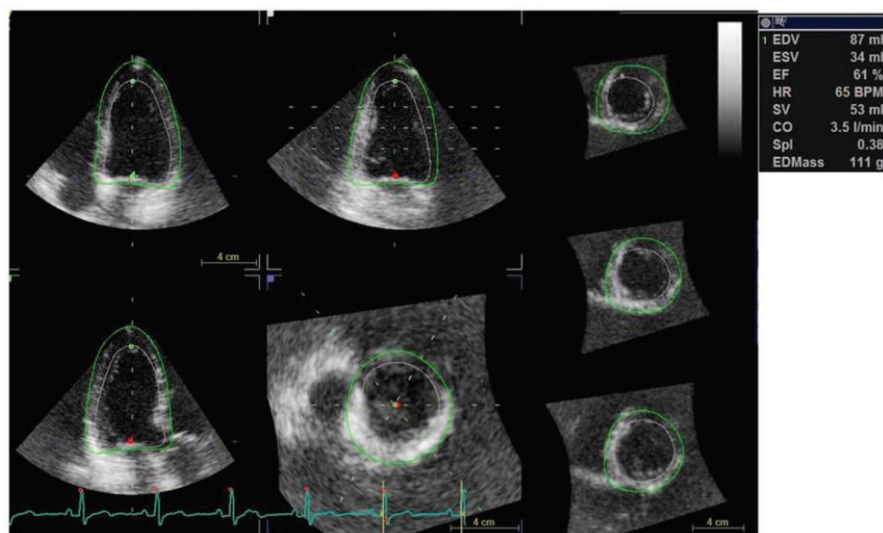


Figure 3. Model of three-dimensional echocardiographic assessment of left ventricular mass, volumes and stroke volume in a hypertensive patient of our study population with elevated left ventricular mass/end-diastolic volume ratio. CO, cardiac output; EDMass, left ventricular mass; EDV, left ventricular end-diastolic volume; EF, left ventricular ejection fraction; ESV, left ventricular end-systolic volume; HR, heart rate; LVM/EDV ratio, left ventricular mass/end-diastolic volume ratio; Spl, sphericity index; SV, stroke volume.

Results: An increased 3D-LVM/EDV ratio identified a higher rate of LV concentric geometry in comparison with 2D-derived relative wall thickness (37 versus 24%, $P=0.03$). Patients with LVM/EDV ratio of 1.22 or more in men and 1.23 or more in women were significantly older, had smaller 3D-LV end-diastolic and end-systolic volumes and higher LV mass index, without difference in ejection fraction. 3D-stroke volume ($P<0.0001$) was lower in patients with elevated LVM/EDV ratio. By a multilinear regression analysis, after adjusting for sex, age, heart rate, mean blood pressure and body mass

index, stroke volume was independently and negatively associated to LVM/EDV ratio (beta=0.55, P<0.0001).

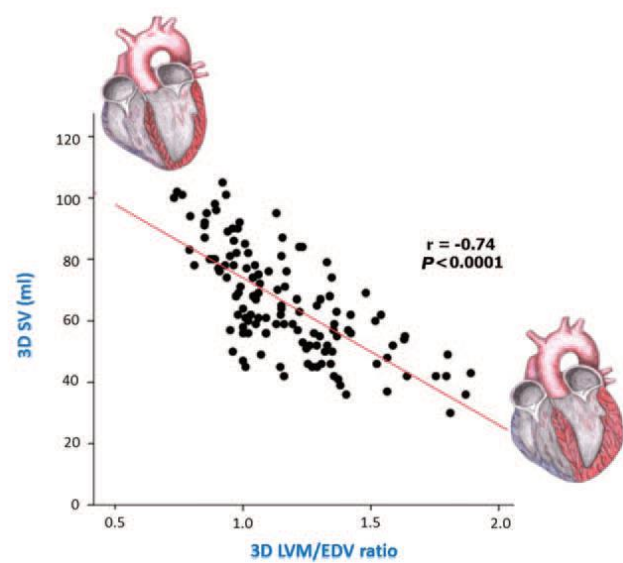


Figure 4. Scatterplot and regression line of individual values of LVM/EDV ratio (x-axis) and corresponding values of stroke volume (SV, y-axis) in the pooled hypertensive population. LVM/EDV ratio, left ventricular mass/end-diastolic volume ratio; SV, stroke volume.

Dependent variable	Covariate	Standardized β coefficient	P value
LV stroke volume (ml)	Female sex	−0.16	<0.01
	Age (years)	−0.23	<0.001
	Heart rate (bpm)	−0.04	0.538
	LVM/EDV ratio	−0.55	<0.0001
	Mean BP (mmHg)	0.02	0.761
	BMI (kg/m ²)	0.07	0.281

Cumulative $R^2 = 0.573$, SEE = 11.5 ml, $P < 0.0001$. LV, left ventricular, LVM/EDV, left ventricular mass/end-diastolic volume ratio.

Table 1. Independent correlates of three-dimensional echocardiographic stroke volume in the pooled hypertensive population by multiple linear regression analysis.

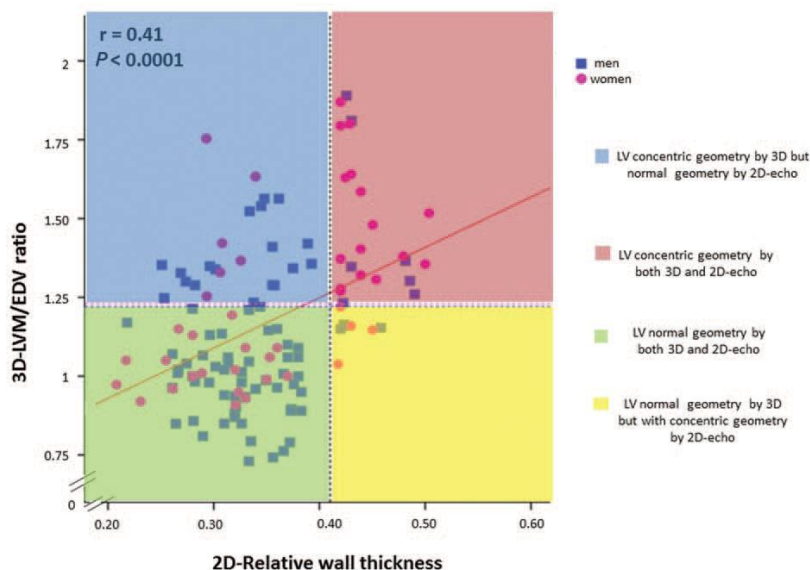


Figure 5. Scatterplot and regression line of individual values of two-dimensional relative wall thickness (x-axis) and corresponding values of three-dimensional left ventricular mass/end-diastolic volume ratio (y-axis) in the pooled hypertensive population. By using the cut-off points of normalcy of relative wall thickness and LVM/EDV ratio, we identified four different LV geometric patterns: LV concentric geometry according to 3D-echo (LVM/EDV ratio of 1.23 or more in women and 1.22 or more in men) but with LV normal geometry by 2D-echo (relative wall thickness <0.41), LV concentric geometry according to both 3D and 2D-echo, LV normal or eccentric geometry according to both 3D and 2D-echo, LV normal or eccentric geometry according to LVM/EDV ratio but with LV concentric geometry according to relative wall thickness. 2D, two-dimensional; 3D, three-dimensional; LV, left ventricular; LVM/EDV ratio, left ventricular mass/end-diastolic volume ratio.

Conclusions: In native hypertensive patients, 3D-echoderived LVM/EDV ratio identifies a higher prevalence of LV concentric geometry than 2D-relative wall thickness. Stroke volume is independently and negatively associated with LVM/EDV ratio and its reduction represents an early marker of myocardial dysfunction in hypertensives with LV concentric geometry.

CHAPTER 4

Impact of left ventricular mass/end-diastolic volume ratio by three-dimensional echocardiography on two-dimensional global longitudinal strain and diastolic function in native hypertensive patients

Background: In hypertensive patients, high LVM/EDV ratio is related to LV dysfunction and myocardial fibrosis ³⁰. We examined the ability of 3D-echo-derived LVM/EDV ratio in identifying early systolic and diastolic dysfunction in relation with LV concentric geometry in native hypertensive patients.

Methods: One-hundred and forty-four newly diagnosed, never treated hypertensive patients underwent 2D-echo, including computation of 2D-derived global longitudinal strain (GLS), and 3D-echo.

Speckle tracking echo of the left ventricle was recorded on 2D images of three consecutive cardiac cycles from the three apical views (long axis, four- and two- chamber) at an approximately equal heart rate. LV cavity was recorded with the narrowest scan and at the lowest possible depth in order to obtain the left ventricle as large as possible on the screen and a frame rate of 40–70 frames/s. The same field depth was maintained for all the views. An interactive software (endocardial-cavity interface traced manually and epicardial tracing generated automatically) rejects segments of poor imaging quality, allowing the observer to manual override its decision by visual assessment. The time of aortic valve closure was marked in the apical long-axis view, as the driving view, and used as reference point in all the

other views. Each of the three apical images was automatically divided into six myocardial segments. Peak negative longitudinal strain was measured from six segments in each of the three apical views (long-axis, four- and two-chamber) and GLS calculated as the average of individual percentage peak strain before aortic valve closure.

The study population was divided into two groups: elevated 3D-LVM/EDV ratio (≥ 1.23 in women and ≥ 1.22 in men), corresponding to LV concentric geometry (n=50), and normal ratio (< 1.23 in women and < 1.22 in men) corresponding to LV normal or eccentric geometry (n=94).

Results: The two groups were comparable for sex, heart rate, body mass index, and blood pressure (BP). Patients with elevated 3D-LVM/EDV ratio were older and had lower GLS ($P < 0.001$) than patients with normal LVM/EDV ratio. Transmitral E/A ratio ($P < 0.0001$) and e' velocity ($P < 0.0001$) were lower, and E/ e' ratio ($P < 0.0001$) higher in patients with elevated LVM/EDV ratio. In the pooled population, LVM/EDV ratio was positively correlated to E/ e' ratio ($r = 0.39$, $P < 0.0001$) and negatively to GLS ($r = -0.29$, $P < 0.001$). By separate multilinear regression analyses, after adjusting for sex, age, heart rate, mean BP and BMI, LVM/EDV ratio – but not 2D-relative wall thickness – was independently associated with E/ e' (beta=0.304, $P = 0.003$) and GLS (beta=-0.501, $P < 0.0001$).

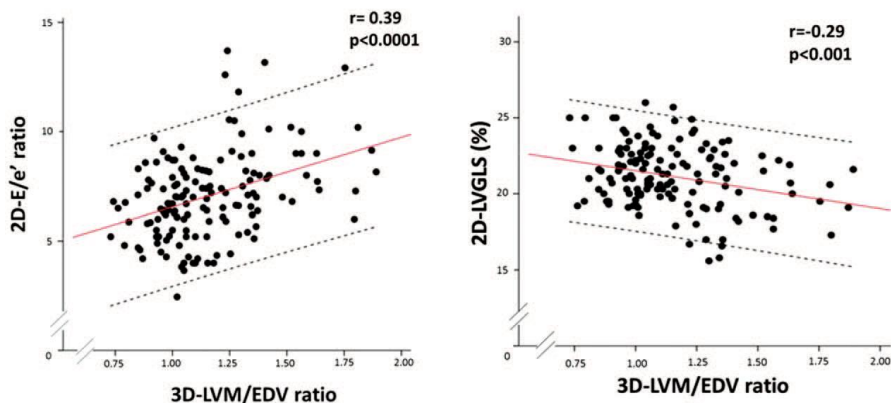


Figure 6. Univariate relation of left ventricular mass/end-diastolic volume ratio with E/e' ratio and global longitudinal strain in the pooled population. On the left, scatterplot, regression line and 95% confidence interval of individual values of 3DLVM/ EDV ratio (x-axis) and corresponding values of 2D-E/e' ratio (y-axis) in the pooled hypertensive population. On the right, scatterplot, regression line and 95% confidence interval of individual values of 3D-LVM/EDV ratio (x-axis) and corresponding values of 2D-LV GLS (y-axis) in the pooled hypertensive population. 2D, two-dimensional; 3D, three-dimensional; GLS, global longitudinal strain; LV, left ventricular; LVM/EDV ratio, LV mass/end-diastolic volume ratio.

Model 1			
Dependent variable	Correlate	Standardized β coefficient	P-value
E/e' ratio	Female sex	0.069	0.416
	Age (years)	0.177	0.056
	BMI (kg/m^2)	0.197	0.017
	Heart rate (bpm)	0.036	0.669
	Mean blood pressure (mmHg)	-0.059	0.470
	3D-LVM/EDV ratio	0.304	0.003
	2D-RWT	0.060	0.507
Model 2			
Dependent variable	Correlate	Standardized β coefficient	P-value
2D-LV GLS (%)	Female sex	0.253	0.004
	Age (years)	0.144	0.125
	BMI (kg/m^2)	-0.094	0.261
	Heart rate (bpm)	0.033	0.694
	Mean blood pressure (mmHg)	-0.144	0.084
	3D-LVM/EDV ratio	-0.501	<0.0001
	2D-RWT	0.145	0.109

Model 1: cumulative $R^2 = 0.240$, SEE = 1.64, $P < 0.0001$. Model 2: cumulative $R^2 = 0.232$, SEE = 1.86%, $P < 0.0001$. GLS, global longitudinal strain; LVM/EDV ratio, LV mass/end-diastolic volume ratio; RWT, relative wall thickness.

Table 2. Multiple linear regression analyses

Conclusion: 3D- echocardiographic assessment of LV concentric geometry allows identifying an early diastolic and longitudinal systolic dysfunction in native hypertensive patients. In particular, 3D-LVM/EDV ratio is

independently associated with both E/e' ratio and GLS.

CHAPTER 5

Interrelation between midwall mechanics and longitudinal strain in newly diagnosed and never-treated hypertensive patients without clinically defined hypertrophy

Background: In hypertensive patients, an impairment of midwall myocardial mechanics was described in presence of LV concentric geometry. Under these circumstances, also LV longitudinal dysfunction was found. Differently oriented but intimately connected myocardial layers characterize the architecture of LV walls ³⁴. Midwall fractional shortening (MFS) is an index which was conceived to examine midwall LV circumferential fibers' function ³⁵. On the other hand, GLS is a feasible echocardiographic parameter, quantifying the motion of LV longitudinal fibers ³. GLS has been described as an early marker of subclinical myocardial mechanics impairment ⁶.

Our aim was to evaluate longitudinal and circumferential systolic function and correlations between these two functional components in newly diagnosed hypertensive patients without clinically defined LV hypertrophy (LVH).

Methods: One hundred and thirty-eight newly diagnosed, never-treated hypertensive patients without LVH and a control group of 105 healthy normotensive individuals underwent two-dimensional and speckle tracking echocardiography. Global longitudinal strain (GLS) was derived (in absolute value) and midwall fractional shortening (MFS) computed. In addition, the hypertensive population was divided into two groups according to GLS:

normal GLS ($\geq 20\%$, $n=94$) and reduced GLS ($<20\%$, $n=44$).

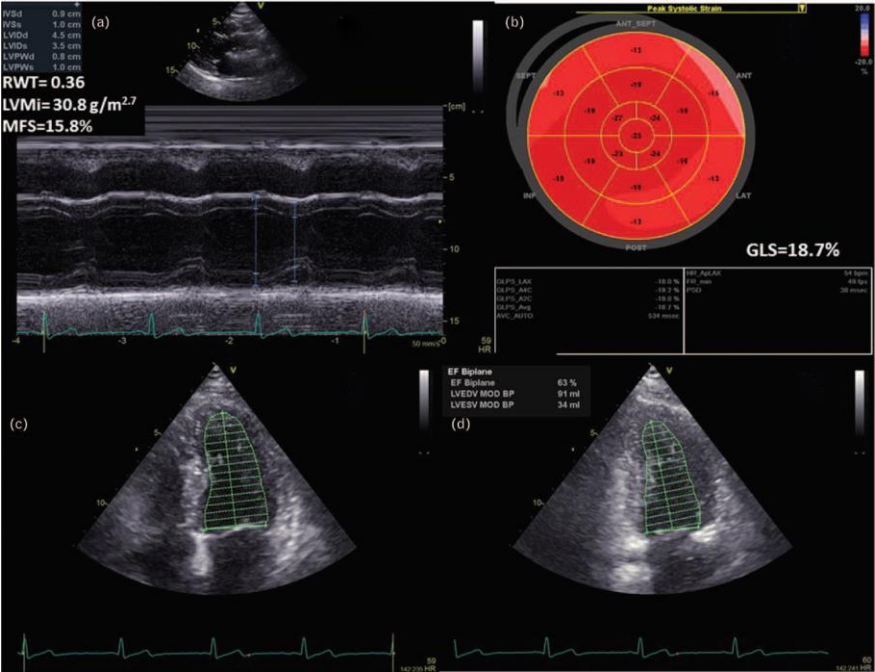


Figure 7. Example of a newly diagnosed, never-treated hypertensive patient of 49 years old (height 1.67 m, weight 85 kg) presenting normal left ventricular geometry and an impairment in both global longitudinal strain and midwall fractional shortening, while left ventricular ejection fraction is still in normal range. Panel (a) shows M-mode-derived left ventricular quantitative analysis and computed midwall fractional shortening. Panel (b) displays bull's eye of left ventricular global longitudinal strain, while panels (c) and (d) present the assessment of biplane left ventricular ejection fraction in both four chamber [panel (c)] and two-chamber [panel (d)] views in the same patient. EF, ejection fraction; GLS, global longitudinal strain; HR, heart rate; IVSd, interventricular septum thickness at end-diastole; IVSs, interventricular septum thickness at end-systole; LV, left ventricular; LVEDV, left ventricular end-diastolic volume; LVESV, left ventricular end-systolic volume; LVIDd, left ventricular internal diameter at end-diastole; LVIDs, left ventricular internal diameter at end-systole; LVMi, left ventricular mass indexed for height powered to 2.7; LVPWd, left ventricular posterior wall thickness at end-diastole; LVPWs, left ventricular posterior wall thickness at end-systole; MFS, midwall fractional shortening.

Results: Hypertensive patients had lower MFS ($P<0.001$) and GLS ($P<0.0001$) than healthy controls. By dividing hypertensive patients according to GLS thresholds of normalcy, MFS was lower in patients with GLS less than 20%

($P<0.0001$) while no significant difference was found in LV geometry, ejection fraction and diastolic parameters in comparison with patients with GLS at least 20%. In the pooled hypertensive population, GLS resulted positively correlated to MFS ($r=0.33$, $P<0.0001$). By a multiple linear regression analysis, after adjusting for female sex, age, body mass index, circumferential end-systolic stress, average e' velocity, ejection fraction and relative wall thickness, MFS remained independently associated with GLS ($b=0.222$, $P<0.005$).

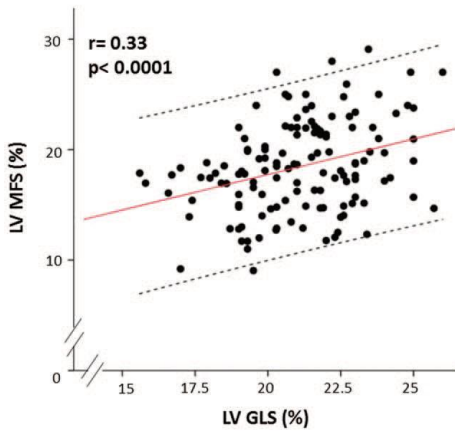


Figure 8. Univariate relation between left ventricular global longitudinal strain and midwall fractional shortening in the pooled population. Scatterplot, regression line and 95% confidence interval of individual values of left ventricular global longitudinal strain (x line) and corresponding values of midwall fractional shortening (y-line) in the pooled hypertensive population. GLS, global longitudinal strain; LV, left ventricular; MFS, midwall fractional shortening.

Dependent variable	Correlate	Standardized β coefficient	P value
GLS (%)	Female sex	0.178	0.042
	Age (years)	-0.212	0.079
	BMI (kg/m ²)	-0.038	0.654
	cESS (kdynes/cm ²)	-0.078	0.437
	Average e' (cm/s)	0.261	0.03
	MFS (%)	0.310	<0.005
	RWT	-0.071	0.486
	LV EF (%)	0.026	0.751

Cumulative $R^2 = 0.21$, SEE = 1.9%, $P < 0.0001$. cESS, circumferential end-systolic stress; EF, ejection fraction; GLS, global longitudinal strain; LV, left ventricular; MFS, midwall fractional shortening; RWT, relative wall thickness; SEE, standard error of estimate.

Table 3. Multiple linear regression analysis.

Conclusion: In newly diagnosed and never-treated hypertensive patients without LVH, an early LV systolic dysfunction is testified by the reduction of both MFS and GLS. These two parameters resulted independently associated after adjusting for several confounders.

CHAPTER 6

Prominent basal and middle strain longitudinal involvement in newly-diagnosed and never treated hypertensive patients without clear-cut hypertrophy

Background: LV GLS can detect an early dysfunction in arterial hypertension, detectable before ejection fraction rection⁸. We investigated regional LV patterns of longitudinal strain (LS) and base-to-apex behavior in newly diagnosed, never-treated hypertensive patients without LV hypertrophy.

Methods: 180 patients affected by arterial hypertension and 115 healthy controls underwent standard echocardiography, including regional LS and GLS assessment (in absolute values). The average LS of six basal (BLS), six middle (MLS), and six apical (ALS) segments and relative regional strain ratio= $[ALS/(BLS + MLS)]$ were also computed.

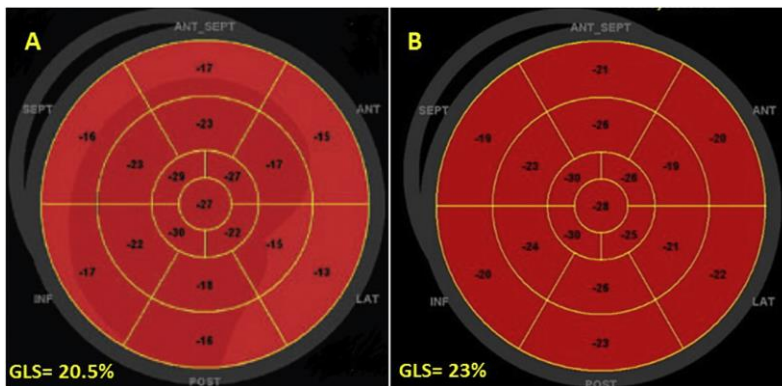


Figure 9. Schema showing an example of a hypertensive patient (Panel A) with GLS values and regional

LS describing relatively reduced BLS and MLS and preserved ALS in comparison with an healthy control subject (Panel B). ALS = apical longitudinal strain, BLS= basal longitudinal strain, GLS = global longitudinal strain, LS = longitudinal strain, MLS = middle longitudinal strain.

Results: The two groups were comparable for sex, age and heart rate. Body mass index, systolic, diastolic and mean BP (all $p < 0.0001$) were higher in hypertensive patients. Despite LV ejection fraction was comparable, GLS, BLS and MLS resulted lower in hypertensive patients (all $p < 0.0001$), without difference in ALS. Relative regional strain ratio resulted higher in hypertensive patients ($p < 0.001$) in comparison to controls. Dividing the hypertensive group according to lower normal values derived from the controls, BLS was able to identify a higher rate of LV dysfunction than GLS. By a multiple linear regression analysis performed in the pooled population after adjusting for age, sex, body mass index, end-systolic stress, relative wall thickness and LV mass index, the association between BLS and mean blood pressure remained significant (β coefficient = -0.42 , $p < 0.0001$), despite the significant impact of male sex. In a similar model, MLS and mean blood pressure resulted also independently associated (β = -0.21 , $p < 0.002$).

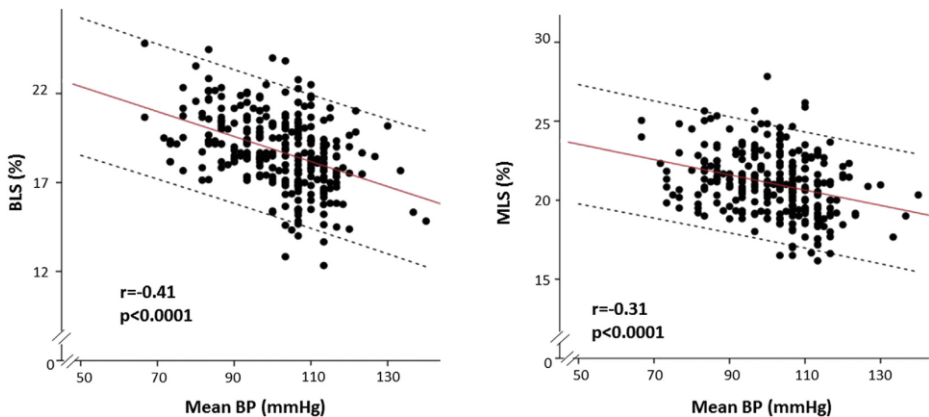


Figure 10. Left panel: univariate relation between mean BP and BLS in the pooled population. Scatterplot, regression line and 95% confidence interval of individual values of mean BP (x-line) and corresponding values of BLS (y line). Right panel: univariate relation between mean BP and MLS in the pooled population. Scatterplot, regression line and 95% confidence interval of individual values of mean BP (x-line) and corresponding values of MLS (y line). BLS = basal longitudinal strain, BP= blood pressure, MLS= middle longitudinal strain.

Dependent variable	Correlate	Standardized β coefficient	p value
Model 1			
BLS (%)	Male sex	-0.243	<0.0001
	Age (years)	0.088	0.123
	Body mass index (kg/m ²)	0.054	0.384
	Mean BP (mmHg)	-0.42	<0.0001
	RWT	-0.028	0.653
	LV mass index (g/m ^{2.7})	-0.054	0.394
	ESS (kdynes/cm ²)	0.059	0.354
Cumulative R ² = 0.25, SEE = 1.8%, p < 0.0001			
Model 2			
MLS (%)	Male sex	0.312	<0.0001
	Age (years)	0.083	0.158
	Body mass index (kg/m ²)	0.025	0.689
	Mean BP (mmHg)	-0.21	<0.002
	RWT	0.019	0.767
	LV mass index (g/m ^{2.7})	-0.076	0.241
	ESS (kdynes/cm ²)	-0.099	0.127
Cumulative R ² = 0.21, SEE = 1.7%, p < 0.0001			
Model 3			
ALS (%)	Male sex	-0.132	0.027
	Age (years)	-0.197	<0.002
	Body mass index (kg/m ²)	-0.002	0.971
	Mean BP (mmHg)	0.033	0.653
	RWT	0.091	0.175
	LV mass index (g/m ^{2.7})	-0.034	0.616
	ESS (kdynes/cm ²)	-0.166	0.016
Cumulative R ² = 0.11, SEE = 3.3%, p < 0.0001			

Table 4. Multiple linear regression analyses.

Conclusions: Despite normal LV ejection fraction, LS dysfunction is detectable in hypertensive patients, mainly involving basal and middle segments, resulting in higher relative regional strain ratio.

CHAPTER 7

Identification of cardiac organ damage in arterial hypertension: insights by echocardiography for a comprehensive assessment

Arterial hypertension, a widespread disease, whose prevalence increases with age, represents a major risk factor for cardiovascular events, causing damage in several organs, including the heart. In this context, echocardiography has a clear and pivotal role, being able to assess cardiac morphology and detect haemodynamic changes induced by this disease. 2018 European Society of Cardiology/European Society of Hypertension guidelines on AH identified main echo parameters such as left ventricular mass, relative wall thickness and left atrial volume, for detecting cardiac organ damage³⁶. The present review highlights the advantage of additional echocardiographic parameters such as diastolic measurement and both thoracic and abdominal aortic dimensions. An overlook on aortic valve should also be suggested to detect aortic regurgitation and stenosis, both frequent complications in hypertensive patients. In this kind of comprehensive assessment, the combination of standard and advanced echocardiography (speckle tracking echocardiography and 3D echocardiography) could be considered to improve the diagnostic accuracy, stratify prognosis and address management in arterial hypertension.

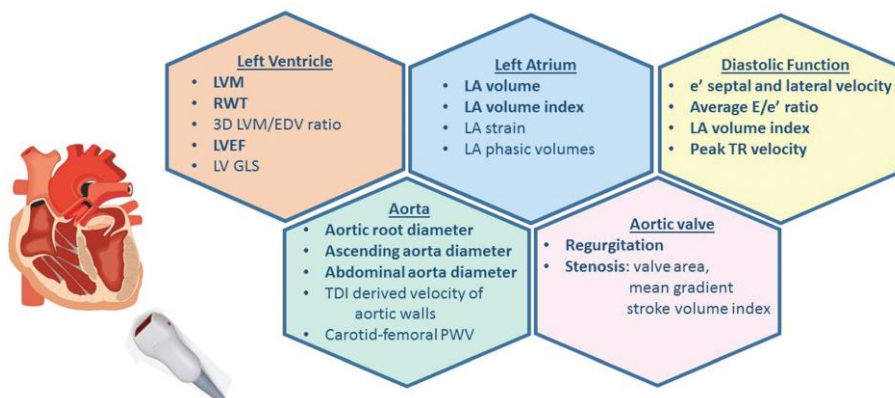


Figure 11. Picture showing the echo parameters useful in the evaluation of the hypertensive patient. In bold letters the parameters that should always be assessed in hypertensive patients. EDV, end-diastolic volume; GLS, global longitudinal strain; LA, left atrium; LV, left ventricular; LVEF, left ventricular ejection fraction; LVM, left ventricular mass; PWV, pulsed wave velocity; RWT, relative wall thickness; TDI, tissue Doppler imaging; TR, tricuspid regurgitation.

The role of echocardiography in the thorough assessment of the hypertensive patient is very useful, as it allows the measurement of several parameters that correlate with organ damage. In addition to LVH and left atrial enlargement identified from current ESC/ESH guidelines on AH to detect cardiac injury³⁶, multiple echocardiographic parameters, such as GLS, left atrial strain and diastolic evaluation could identify an early heart impairment³⁷. The evaluation of LV and left atrial function, rather than the simple measure of their dimensions, has given promising results in early detection of cardiac dysfunction, which might help identifying patients that can benefit from a more aggressive treatment and a closer follow-up^{37, 38}. Also the evaluation of diastolic dysfunction is extremely important, because it can occur before the development of LV geometry changes³⁹. Moreover, in a complete overview on AH-induced cardiac impairment the assessment of aortic dimension and aortic valve function should not be overlooked^{40, 41}. In this context, the combination of standard and advanced

echocardiographic techniques should be carefully considered to diagnose subclinical cardiac organ damage, stratify prognosis and address management at the best.

In this view, based on a preliminary clinical assessment, the echocardiographic evaluation could gather the maximum of relevant information on heart and aorta by influencing patients' treatment, and also establishing correct timing of follow-up. Accordingly, under well-defined circumstances, echocardiography could present even a valuable cost/effectiveness ratio in hypertensive patients.

CHAPTER 8

Mechano-energetic efficiency as a predictor of left ventricular systolic dysfunction in hypertensive patients with optimal blood pressure control

Background: We aimed at analyzing possible predictors of LV ejection fraction (LVEF) reduction, including indexed mechano-energetic efficiency (MEEi), a well-recognized echo-derived parameter of LV performance⁴², in a hypertensive population with optimal blood pressure control in a long-term follow-up.

Methods: The study population included 5,673 hypertensive patients, from The Campania Salute Network, with normal baseline LVEF ($\geq 50\%$) and no prevalent cardiovascular disease. Patients were followed-up for about 5 years and those developing LVEF impairment ($\text{LVEF} < 50\%$ or a reduction of 10% compared to baseline) were compared to patients with persistently normal LVEF.

Results: Optimal blood pressure control was achieved in about 80% of patients. Patients who experienced LVEF reduction were 2.41%. They were older ($p < 0.0001$), more often diabetic ($p < 0.001$), presented higher LV mass index and carotid intima-media thickness (both $p < 0.0001$), while lower MMEi ($p = 0.037$) at baseline, and developed a higher prevalence of cardiovascular events ($p < 0.0001$) in comparison to patients with normal LVEF. A logistic regression analysis, performed by excluding patients who experienced cardiovascular events, demonstrated that independent predictors of LVEF reduction were heart rate, LV mass index and the lowest

MMEi quartile, the latter being a stronger predictor (Odds Ratio 1.81, $p<0.0001$) than both heart rate and LV mass index. ROC curves showed that the model including MMEi had higher accuracy than the model without MEEi in predicting LVEF reduction (AUC 0.739 vs. 0.682, $p<0.0001$).

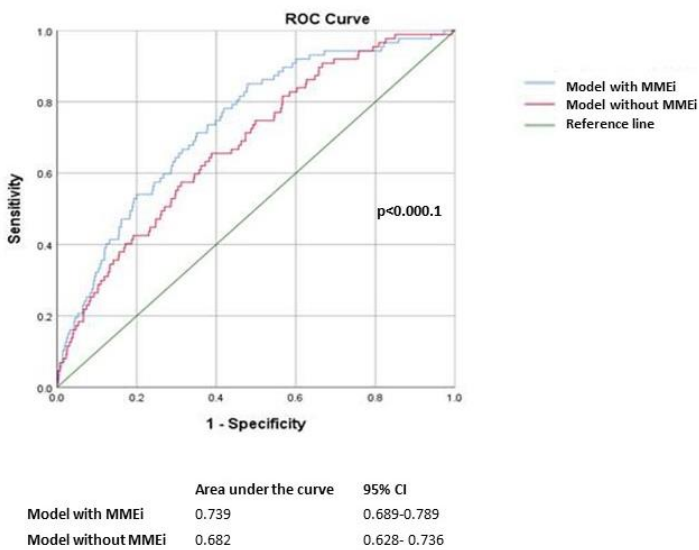


Figure 12. ROC curves for predicted probability assessed according to two models, the first one including all parameters present in table 4 including MMEi and the second one including the same parameters without MMEi. The model including MMEi predicted LVEF reduction better than the model without this parameter. MEEi= indexed mechano-energetic efficiency.

Conclusions: Lower values of MEEi at baseline identified hypertensive patients more liable to develop LVEF reduction. In hypertensive setting, MEEi evaluation improved prediction of LV systolic dysfunction during long-term follow-up.

Part II

Advanced ultrasound cardiac imaging in other cardiovascular diseases

CHAPTER 9

Strain-oriented strategy for guiding cardioprotection initiation of breast cancer patients experiencing cardiac dysfunction

Background: Cancer therapy progressively prolongs survival in oncologic diseases. Nevertheless, it may expose patients to life-threatening complications involving the cardiovascular system. Thus, cardiotoxicity may become one of the main determinants of quality-of-life impairment and mortality in this specific population^{43, 44}. Cancer therapy-related cardiac dysfunction (CTRCD) can be due to different kinds of treatment: anthracyclines provoke a dose-cumulative myocardial damage with irreversible cellular necrosis (Type I cardiotoxicity), while other agents, such as trastuzumab, lead to a non-dose-related but reversible cardiac impairment (Type II cardiotoxicity)⁴⁴. The sequential or concurrent use of these two different types of agents may increase myocardial injury and CTRCD is often the result of the combined detrimental effect of the two therapies. A timely initiation of cardioprotective treatment for CTRCD is pivotal to continue the ongoing CT till completion and reduce the risk of overt heart failure⁴⁵. Cardiac treatment of CTRCD is currently guided by 2D echocardiographic evaluation of LVEF⁴⁶. However, LVEF is affected by several limitations including its load-dependence, the need of geometric assumption for its calculation and, above-all, its substantial biological (day-to-day) variability that makes subtle changes often doubtful and questionable. As an alternative, GLS, easily obtainable by speckle tracking

echocardiography, has shown optimal feasibility and temporal reproducibility and its changes may precede LVEF reduction in the general population and in oncologic patients as well⁴⁷.

This study assessed the impact of the strain-guided therapeutic approach on CTRCD and rate of cancer therapy interruption in breast cancer.

Methods: We enrolled 116 consecutive female patients with HER2-positive breast cancer undergoing a standard protocol by epirubicine + cyclophosphamide followed by paclitaxel + trastuzumab. Coronary artery, valvular and congenital heart disease, heart failure, primary cardiomyopathies, permanent or persistent atrial fibrillation, and inadequate echo-imaging were exclusion criteria. Patients underwent an echo-Doppler exam with determination of LVEF and global GLS at baseline and every 3 months during cancer therapy. All patients developing subclinical (GLS drop >15%) or overt CTRCD (LVEF reduction <50%) initiated cardiac treatment (ramipril + carvedilol).

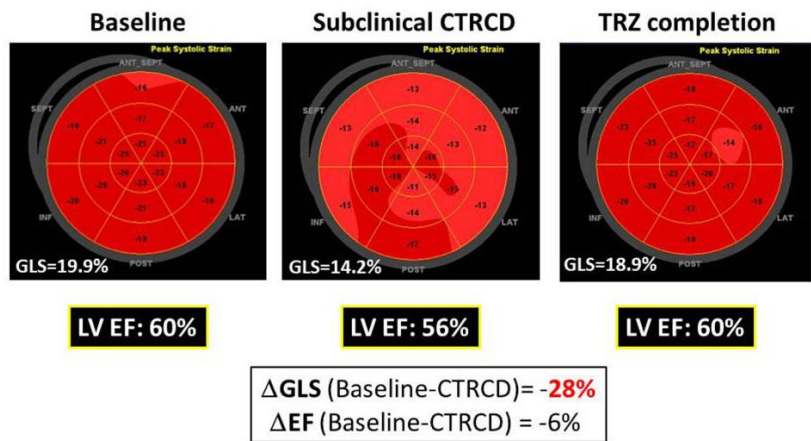


Figure 13. Clinical case of a patients developing subclinical CTRCD at the XI TRZ cycle but completing successfully TRZ thanks the timely cardioprotective treatment. Bull's eyes of GLS at baseline (left), at the time of subclinical CTRCD (mid), and at cancer therapy completion (right). CTRCD, cancer therapy-related cardiotoxicity; EF, ejection fraction; GLS, global longitudinal strain; TRZ, trastuzumab.

Results: In the 99.1% (115/116) of patients successfully completing chemotherapy, GLS and LVEF were significantly reduced and E/e' ratio increased at therapy completion. Combined subclinical and overt CTRCD was diagnosed in 27 patients (23.3%), 8 at the end of epirubicine + cyclophosphamide and 19 during trastuzumab courses. Of these, 4 (3.4%) developed subsequent overt CTRCD and interrupted chemotherapy. By cardiac treatment, complete LVEF recovery was observed in two of these patients and partial recovery in one. These patients with LVEF recovery restarted and successfully completed chemotherapy. The remaining patient, not showing LVEF increase, permanently stopped chemotherapy. The other 23 patients with subclinical CTRCD continued and completed chemotherapy.

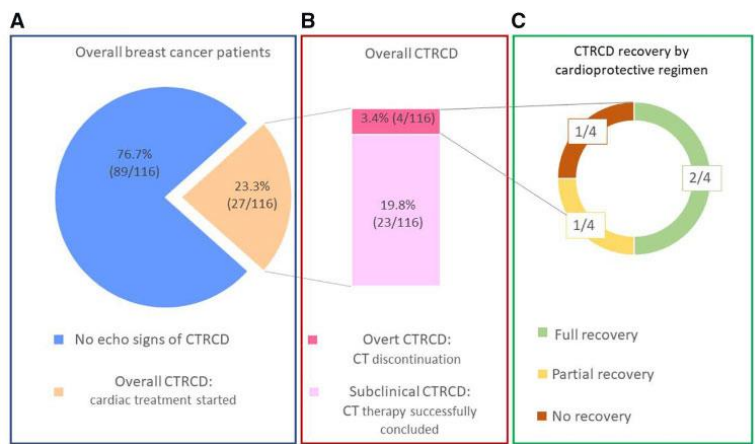


Figure 14. Picture of the study population. (A) Overall breast cancer population, (B) CTRCD (both subclinical and clinical) population, and (C) CTRCD recovery after cardioprotective regimen. CTRCD, cancer therapy-related cardiac dysfunction.

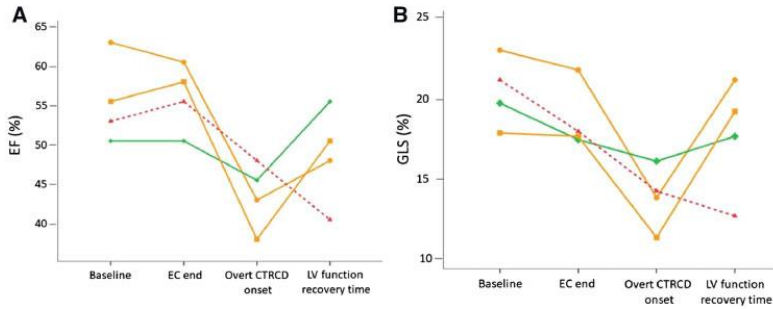


Figure 15. Behaviour of EF (A) and GLS (B) at EC end, at the time of overt CTRCD onset (during TRZ) and at the time of LV function recovery in the individual patients developing overt CTRCD. Solid green lines indicate patients with full LV function recovery thanks cardioprotective regimen (at 60 and 95 days, respectively); solid orange lines indicate patient with partial LV function recovery thanks cardioprotective regimen (at 120 days). Dotted red lines indicate patient without LV function recovery (after 51 days after interrupting chemotherapy) and forced to permanently stop chemotherapy. CTRCD, cancer therapy-related cardiac dysfunction; EC, epirubicine þ cyclophosphamide; EF, ejection fraction; GLS, global longitudinal strain; LV, left ventricular.

Conclusions: These findings highlight the usefulness of ‘strain oriented’ approach in reducing the rate of overt CTRCD and chemotherapy interruption by a timely cardioprotective treatment initiation.

CHAPTER 10

Prominent longitudinal strain reduction of left ventricular basal segments in treatment-naive Anderson-Fabry disease patients

Background: Anderson-Fabry disease (AFD) is a rare X-linked metabolic disorder due to deficiency in lysosomal enzyme activity of α -galactosidase A, resulting in pathological accumulation of glycosphingolipids in several tissues and a multi-organ progressive dysfunction⁴⁸. AFD cardiomyopathy has been described in both genders, in a specific late-onset cardiac variant, and is largely associated with LV hypertrophy (LVH), impaired diastolic function, and late systolic dysfunction^{49, 50}. Among the different myocardial deformation components, GLS has shown the best ability in detecting subclinical cardiac involvement. The regional distribution of LS has also shown typical patterns in different types of LVH, mainly in cardiac amyloidosis, which is characterized by a typical LS reduction in basal LV segments, with a relative apical sparing^{51, 52}. A reduction of GLS has also been associated with myocardial fibrosis as identified by native T1 mapping in early AFD⁵³, but little is known about the regional LS distribution in the subclinical stages of AFD cardiomyopathy. The present study was designed to investigate specific regional patterns of LS and base-to-apex behaviour of longitudinal deformation in treatment-naive AFD patients.

Methods: Twenty-three consecutive AFD patients at diagnosis and 23 healthy controls without cardiovascular risk factors and matched for age and sex to the patients, underwent a comprehensive evaluation of target organs. An echo-Doppler exam, including determination of regional and global LS

strain (GLS) was obtained. The average LS of 6 basal (BLS), 6 middle (MLS), and 5 apical (ALS) segments and relative regional strain ratio [ALS/(BLS þ MLS)] were also calculated.

Results: Ejection fraction and diastolic indices did not differ between the two groups. LV mass index was greater in AFD ($P < 0.01$). GLS ($P = 0.006$), BLS ($P < 0.0001$), and MLS ($P = 0.003$), but not ALS, were lower in AFD patients and relative regional strain ratio was higher in AFD ($P < 0.01$) than in controls. These analyses were confirmed separately in the two genders and even after excluding patients with wall hypertrophy. By subdividing AFD patients according to lysoGB3 levels, 9 patients with lysoGB3 ≥ 1.8 ng/L had lower ALS compared to 11 patients with lysoGB3 < 1.8 ng/L ($P < 0.01$).

	Control subjects (n = 23)	AFD patients (n = 23)	P-value
Global longitudinal strain (%)	23.1 \pm 1.8	21.7 \pm 1.6	0.006
Basal segments longitudinal strain (%)	20.9 \pm 1.2	18.0 \pm 2.0	<0.0001
Mid segments longitudinal strain (%)	22.0 \pm 1.7	20.5 \pm 1.4	0.003
Apical segments longitudinal strain (%)	26.6 \pm 3.6	26.5 \pm 3.8	0.92
Relative regional strain ratio	0.62 \pm 0.07	0.69 \pm 0.11	<0.01
Regional longitudinal strain			
Inferior lateral wall-basal (%)	21.5 \pm 2.1	19.4 \pm 3.8	<0.02
Inferior lateral wall-mid (%)	20.6 \pm 2.3	19.2 \pm 2.6	0.06
Anterior septal wall-basal (%)	19.7 \pm 2.8	17.7 \pm 3.6	0.04
Anterior septal wall-mid (%)	23.8 \pm 3.9	23.5 \pm 3.1	0.74
Posterior septal wall-basal (%)	20.7 \pm 1.0	17.2 \pm 3.7	<0.0001
Posterior septal wall-mid (%)	21.7 \pm 2.5	21.5 \pm 3.7	0.78
Lateral wall-basal (%)	21.0 \pm 3.1	16.9 \pm 2.4	<0.0001
Lateral wall-mid (%)	21.4 \pm 3.4	18.2 \pm 2.4	<0.001
Inferior wall-basal (%)	21.9 \pm 2.5	19.9 \pm 3.3	<0.02
Inferior wall-mid (%)	23.4 \pm 2.4	22.9 \pm 2.8	0.50
Anterior wall-basal (%)	20.6 \pm 2.2	17.2 \pm 3.3	<0.0001
Anterior wall-mid (%)	20.9 \pm 2.7	18.0 \pm 3.3	0.003
Anterior apex (%)	25.3 \pm 4.5	23.9 \pm 5.9	0.36
Inferior apex (%)	28.6 \pm 4.6	29.4 \pm 5.4	0.67
Septal apex (%)	27.7 \pm 4.5	28.4 \pm 3.1	0.52
Lateral apex (%)	25.1 \pm 3.1	24.7 \pm 3.6	0.88
Apical cap (%)	26.4 \pm 3.2	26.2 \pm 3.3	0.90

Table 6. Regional and global longitudinal strain.

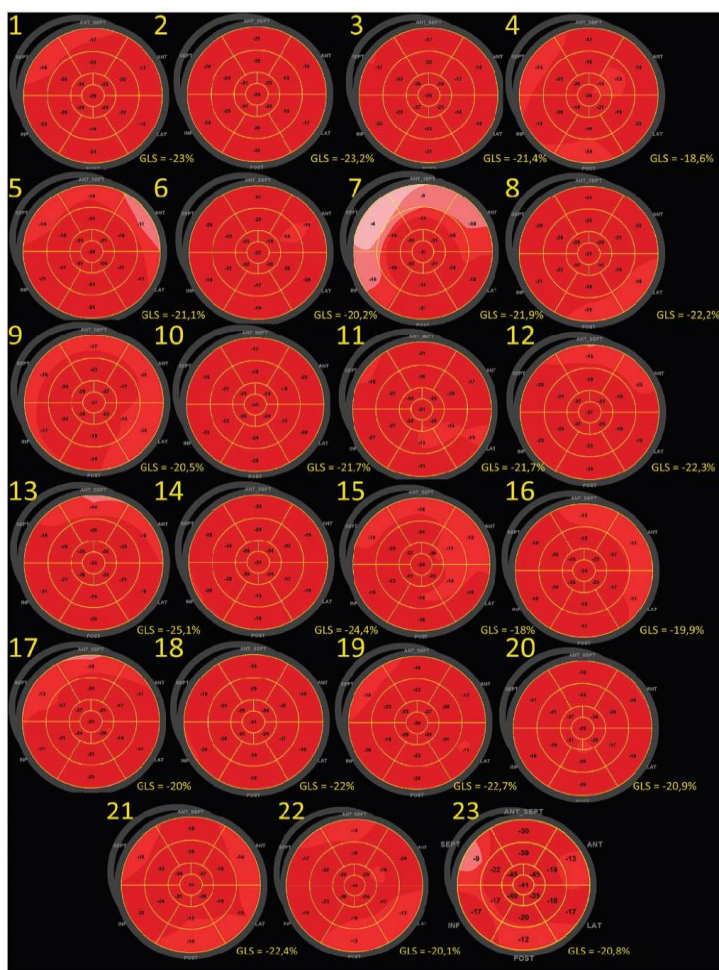


Figure 16. Polar maps (bull's eyes) of regional longitudinal strain (LS) in individual AFD patients, listed in the same order of Table 2. Four distinct patterns are recognizable: (1) normal or near normal regional LS (Patients n 2, 3, 6, 10, 14, 18, and 20); (2) LS reduction in septal and anterior regions (Patients n 1, 5, 7, 12, 13, 17 and 19); (3) LS reduction in both septal/anterior and infero-lateral regions (Patients n 4, 9, 15, 16, 21, 22 and 23); (4) LS reduction in infero-lateral region (Patients n 8 and 11). Independent of the involved region, LS of basal segments appears to be more impaired in the majority of patients with abnormal LS patterns.

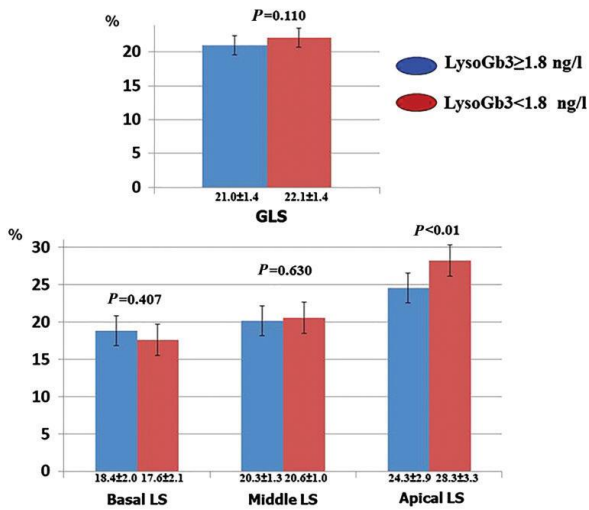


Figure 17. Global and regional longitudinal strain for basal, mid, and apical level according to lysoGP3 (values >1.80 are considered elevated).

Conclusions: In naive AFD patients, we observed an early reduction of LV LS, involving mainly LV basal myocardial segments. Nevertheless, the association found between the higher lysoGB3 levels and the lower apical cap LS demonstrates that apical segments LS, despite still normal, is not spared at diagnosis.

CHAPTER 11

Left ventricular diastolic abnormalities other than valvular heart disease in antiphospholipid syndrome: An echocardiographic study

Background: Antiphospholipid syndrome (APS) can be primary or secondary to other autoimmune disorders⁵⁴. Besides valvular heart disease and coronary artery disease (CAD)^{55, 56}, little is known about the impact of APS on LV function.

Methods: After excluding CAD, relevant valvular heart disease and heart failure, 69 patients (mean age = 43.9 years, 40 with primary and 29 with secondary APS) were assessed by echo-Doppler. Sixty-nine healthy controls, matched for age and sex, formed the control group. APS was diagnosed in presence of at least one clinical criteria and one confirmed laboratory criteria, including lupus anticoagulant titre. The adjusted global APS score (aGAPSS), derived from the combination of risk factors for thrombosis and autoimmune-antibody profile was calculated.

Results: Patients had similar blood pressure and heart rate, but higher body mass index than controls. LV mass index ($p = 0.007$) and left atrial volume index ($p < 0.01$) were greater, while early diastolic velocity (e') was lower ($p=0.003$) and E/e' higher ($p=0.007$) in APS. Primary APS patients had lower E/A ratio and e' velocity compared to both controls and secondary APS, while E/e' ratio was higher in secondary APS than in controls. APS patients with diastolic dysfunction were older but did not differ for risk factors prevalence from those with normal/indeterminate diastolic function. In the pooled APS,

Lupus anticoagulant positivity was independently associated with e' velocity and E/e' ratio after adjusting for age, body mass index and aGAPSS in separate multivariate models.

Variable	Group 1 Controls (n = 69)	p value group 1 vs group 2	Group 2 Primitive APS patients (n = 39)	p value group 2 vs group 3	Group 3 Secondary APS patients (n = 29)	p value group 1 vs group 3	Cumulative p value
Relative wall thickness	0.33 ± 0.05	1.000	0.35 ± 0.07	0.865	0.34 ± 0.07	1.000	0.265
LV mass (g)	121.6 ± 27.0	<0.001	145.9 ± 41.9	0.09	127.9 ± 37.5	1.000	<0.001
LV Mass Index (g/m ^{2.7})	31.5 ± 6.7	<0.001	36.5 ± 10.3	0.09	33.7 ± 8.6	1.000	<0.001
LV EF (%)	63.0 ± 5.0	1.000	63.0 ± 6.0	1.000	62.8 ± 5.3	1.000	0.979
LV GLS (%)	-21.5 ± 5.7	1.000	-21.3 ± 2.4	1.000	-20.9 ± 2.6	1.000	0.868
Transmitral E velocity (cm/s)	0.80 ± 0.17	0.015	0.71 ± 0.14	0.018	0.82 ± 0.16	1.000	0.007
Transmitral E/A ratio	1.30 ± 0.5	<0.005	1.02 ± 0.4	0.007	1.36 ± 0.4	1.000	0.002
E velocity DT (msec)	199.7 ± 52.5	0.557	213.1 ± 51.0	1.000	202.8 ± 37.1	1.000	0.412
Average e' (cm/s)	12.5 ± 3.4	<0.0001	9.5 ± 2.8	0.008	12.2 ± 3.2	1.000	<0.0001
E/e' ratio	6.6 ± 1.5	0.017	8.0 ± 2.9	1.000	7.6 ± 3.1	0.266	0.014
LA volume index (ml/m ²)	23.8 ± 6.1	0.265	25.8 ± 5.1	0.721	27.5 ± 6.4	<0.01	0.014
sPAP (mm Hg)	26.3 ± 6.6	1.000	27.8 ± 7.4	1.000	26.6 ± 10.0	1.000	0.667

Table 5. ANOVA analysis among controls, primary and secondary APS.

Conclusion: In APS, LV diastolic abnormalities are detectable. They are more pronounced in primary APS and independently associated with lupus anticoagulant positivity.

CHAPTER 12

Cardiac Manifestations of Antiphospholipid Syndrome: Clinical Presentation, Role of Cardiac Imaging, and Treatment Strategies

APS is an autoimmune disorder characterized by the presence of antiphospholipid antibodies, vascular thrombosis (venous, arterial, or small vessels), and/or pregnancy morbidity⁵⁴. Diagnosis of APS is based on the presence of at least one clinical criterion (thrombotic events or pregnancy morbidity) and at least one of the laboratory criteria (persistently medium/high titer immunoglobulin G [IgG]/ immunoglobulin M [IgM] anticardiolipin antibodies, and/or medium/high titer IgG/IgM anti- β 2-glycoprotein I antibodies, and/or a positive lupus anticoagulant test), confirmed after repetition at least 12 weeks apart. The clinical spectrum of APS encompasses additional (extra criteria) clinical manifestations, including cardiac diseases⁵⁴.

Heart involvement may become evident as a consequence of direct (autoimmune-mediated) or indirect (thrombosis) mechanisms, and include valve heart disease (vegetations and/or thickening associated with functional abnormalities) and intracardiac thrombosis, coronary, and vascular accelerated atherosclerosis, along with ischemic heart disease. APS can also cause pulmonary arterial hypertension, left ventricular dysfunction, and heart failure^{55, 56}. This review describes the major cardiac manifestations of APS and illustrates the role of cardiac imaging for diagnosing subclinical and overt heart involvement and addressing management of these patients. The possible role of therapeutic strategies in cardiac manifestations of APS is also discussed.

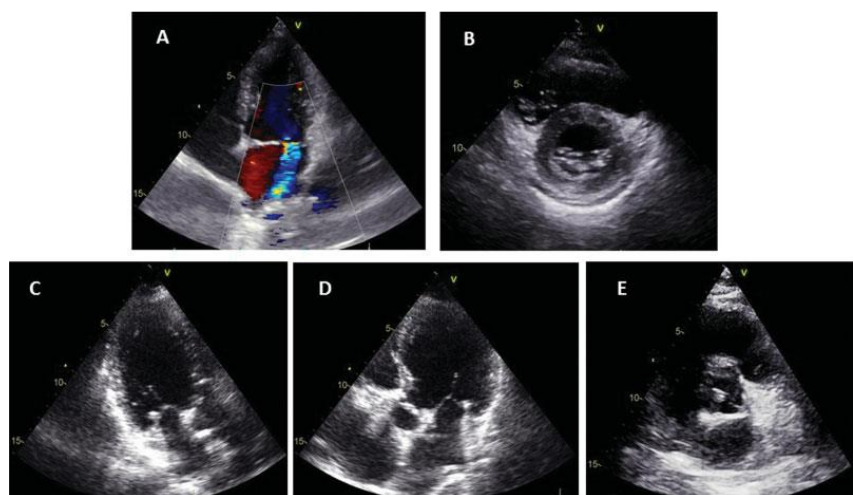


Figure 18. TTE of different APS patients with valvular heart disease. (A) Moderate mitral regurgitation. (B) Mitral valve thickening associated to mild pericardial effusion. (C and D) Calcifications on the posterior mitral leaflet and aortic cusps are presented. (E) Calcifications of aortic leaflets. APS, antiphospholipid syndrome; TTE, transthoracic echocardiography.



Figure 19. TEE of a woman with SLE and APS. TEE allows identifying a Libman–Sacks endocarditis of the aortic valve (yellow arrow) and a thrombus in right atrial cavity (red arrow). AO, aorta; APS, antiphospholipid syndrome; LA, left atrium; RA, right atrium; SLE, systemic lupus erythematosus; TEE, transesophageal echocardiography.

Antiphospholipid syndrome encompasses a wide spectrum of thrombotic and non-thrombotic cardiac manifestations. The correct diagnosis is crucial for adequate antithrombotic treatment, in order to avoid overtreatment and reduce the thrombotic burden of those patients at truly high risk. The mainstream role of cardiovascular imaging in this setting is recognized and

should be strongly promoted to identify subclinical coronary and vascular atherosclerosis and detect valve abnormalities, cardiac dysfunction, ischemic disease, and thromboembolic events. Preventive strategies should be balanced on the basis of global cardiovascular risk profile.

CHAPTER 13

Impaired Right and Left Ventricular Longitudinal Function in Patients with Fibrotic Interstitial Lung Diseases

Background: LV and right ventricular (RV) dysfunction is recognized in idiopathic pulmonary fibrosis (IPF)⁵⁷. Little is known about cardiac involvement in non-idiopathic pulmonary fibrosis (no-IPF). This issue can be explored by advanced echocardiography.

Methods: Thirty-three clinically stable and therapy-naive fibrotic IPF and 28 no-IPF patients, and 30 healthy controls were enrolled. Exclusion criteria were autoimmune systemic diseases, coronary disease, heart failure, primary cardiomyopathies, chronic obstructive lung diseases, pulmonary embolism, primary pulmonary hypertension. Lung damage was evaluated by diffusion capacity for carbon monoxide (DLCOsb). All participants underwent an echo-Doppler examination including 2D GLS of both ventricles and 3D echocardiographic RV ejection fraction (RVEF).

Results: We observed LV diastolic dysfunction in IPF and no-IPF, and LV GLS but not LV EF reduction only in IPF. RV diastolic and RV GLS abnormalities were observed in IPF versus both controls and no-IPF. RV EF did not differ significantly between IPF and no-IPF. DLCOsb and RV GLS were associated in the pooled pulmonary fibrosis population and in the IPF subgroup ($\beta = 0.708$, $p < 0.001$), independently on confounders including pulmonary arterial systolic pressure.

Variable	IPF (n = 33)	No-IPF (n = 28)	p^a	Controls (n = 30)	p^b	p^c
Standard Echo-Doppler						
RV basal tract diameter (mm)	39.8 ± 4.5	38.3 ± 5.7	0.574	35.9 ± 7.0	0.028	0.278
RV mid track diameter (mm)	32.6 ± 5.9	30.7 ± 5.9	0.387	29.3 ± 4.6	0.051	0.579
RV longitudinal diameter (mm)	64.2 ± 7.7	61.4 ± 7.6	0.391	61.5 ± 8.7	0.409	0.998
TAPSE (mm)	20.9 ± 2.9	22.4 ± 3.4	0.165	23.4 ± 3.2	0.007	0.453
Tricuspid E/A ratio	0.88 ± 0.36	0.91 ± 0.21	0.958	1.20 ± 0.30	<0.001	<0.002
PASP (mmHg)	39.6 ± 19.8	37.2 ± 8.1	0.514	26.7 ± 4.6	0.002	0.047
STE and 3D Echocardiography						
RV GLS (%)	20.0 ± 2.6	22.1 ± 2.8	<0.05	24.2 ± 4.4	<0.001	<0.05
3D RV EDV (mL)	85.5 ± 2.0	81.3 ± 34.7	0.911	78.6 ± 36.0	0.779	0.959
3D RV ESV (mL)	40.6 ± 15.9	38.8 ± 16.6	0.928	33.3 ± 18.3	0.320	0.495
3D SV (mL)	44.9 ± 18.5	42.6 ± 20.6	1.0	45.4 ± 19.0	1.0	1.0
3D RV EF (%)	50.5 ± 9.9	50.9 ± 7.6	0.987	59.1 ± 6.9	<0.002	<0.002

Table 7. Standard and advanced echo-Doppler parameters of the right ventricle.

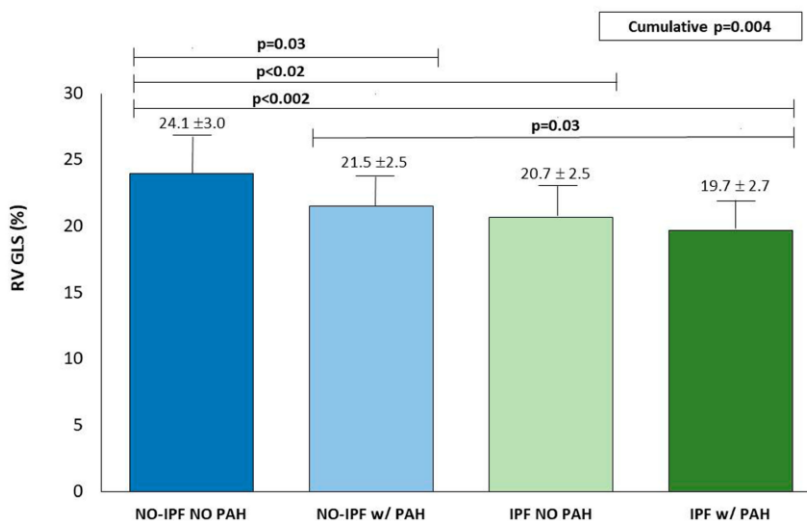


Figure 20. Behavior of RV GLS (mean ± SD) in no-IPF and IPF without and with PAH. RV GLS is significantly lower in IPF with or without pulmonary arterial hypertension (PAH) in comparison with both no-IPF groups.

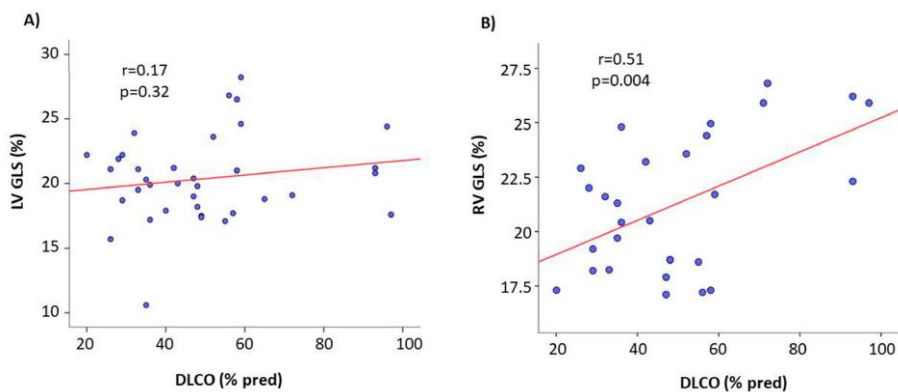


Figure 21. Scatterplot and regression line of the relation between DLCO and both LV GLS and RV GLS in the pooled interstitial lung diseases population. The relation of RV GLS—but not of LV GLS—is significant.

		In the pooled ILDs population ^a		In IPF subgroup ^b		In no-IPF subgroup ^c	
Dependent variable	Covariate	B coefficient	<i>p</i>	B coefficient	<i>p</i>	B coefficient	<i>p</i>
RV GLS	BMI	-0.186	0.214	-0.267	0.139	-0.227	0.339
	HR	-0.027	0.851	-0.045	0.794	-0.190	0.536
	PASP	-0.053	0.712	-0.203	0.239	-0.304	0.277
	DLCO _{sb}	0.583	<0.0001	0.708	<0.001	0.219	0.464

(a) Cumulative $R^2 = 0.575$, SEE = 2.22%, $p < 0.007$; (b) Cumulative $R^2 = 0.729$, SEE = 1.91 %, $p = 0.009$; (c) Cumulative $R^2 = 0.729$, SEE = 1.91 %, $p = 0.009$; ILDs = interstitial lung diseases; IPF = idiopathic pulmonary fibrosis; DLCO_{sb}= single-breath lung diffusion capacity of carbon monoxide; PASP = pulmonary arterial systolic pressure; RV = right ventricular; GLS = Global longitudinal strain; SEE = standard error estimated.

Table 8. Multiple linear regression analyses.

Conclusion: Our data highlight the unique diagnostic capabilities of GLS in distinguishing early cardiac damage of IPF from no-IPF patients.

CHAPTER 14

Cardiopulmonary exercise testing and echocardiographic exam: a useful interaction

Cardiopulmonary exercise test (CPET) is a functional assessment that helps to detect disorders affecting the system involved in oxygen transport and utilization through the analysis of the gas exchange during exercise. The clinical application of CPET is various, including training prescription, evaluation of treatment efficacy and outcome prediction in a broad spectrum of conditions⁵⁸. Furthermore, in patients with shortness of breath it provides pivotal information to bring out an accurate differential diagnosis between physical deconditioning, cardiopulmonary disease and muscular diseases⁵⁹. Modern software allows the breath-by-breath analysis of the volume of oxygen intake, volume of carbon dioxide output and expired air. Through this analysis, CPET provides a series of additional parameters (peak volume of oxygen intake, ventilatory threshold, volume of expired air/ volume of carbon dioxide output slope, end-tidal carbon dioxide exhaled) that characterize different patterns, helping in diagnosis process⁶⁰. Limitations to the routine use of CPET are mainly represented from the lack of measurement standardization and limited data from randomized multicentric studies. The integration of CPET with exercise stress echocardiography has been recently introduced in the clinical practice by integrating the diagnostic power offered by both the tools^{61, 62}. This combined approach has been demonstrated to be valuable for diagnosing several cardiac diseases, including heart failure with preserved or reduced ejection fraction, cardiomyopathies, pulmonary arterial hypertension,

valvular heart disease and coronary artery disease⁶³. On the grounds of recognized evidence, it is conceivable that CPET data combined with clinical, laboratory and echocardiographic measurements could very efficiently stratify prognosis in patients with cardiac diseases.

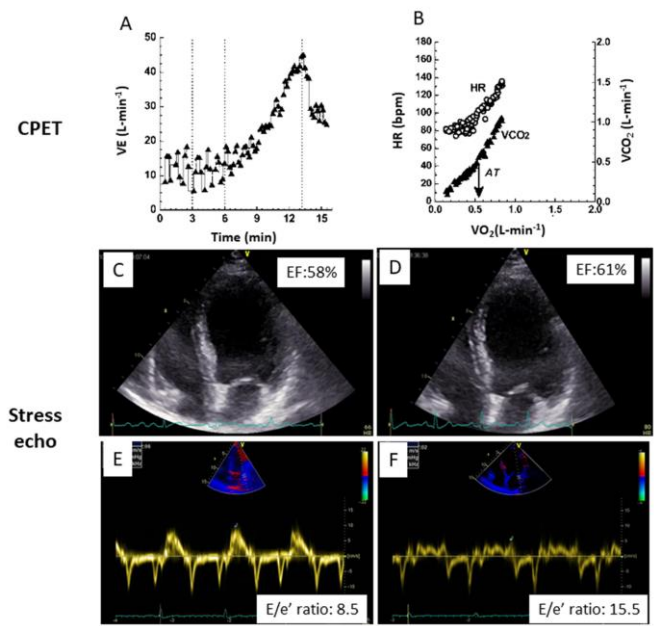


Figure 22. Illustrative clinical case of combined CPET and stress echo approach in a patient affected by HFpEF. CPET analysis shows clear oscillatory patterns of minute ventilation (VE) (a) and reduced VE/VCO₂ ratio (b). Echocardiographic exam at rest shows a preserved ejection fraction (c) and an E/e' ratio in the normal range (e). At peak exercise the ejection fraction is normal (d) but E/e' appears to be pathologically increased (f).

CHAPTER 15

Global longitudinal strain is a hallmark of cardiac damage in mitral regurgitation: the Italian arm of the European Registry of mitral regurgitation

Background: The search for reliable cardiac functional parameters is crucial in patients with mitral regurgitation (MR). In the Italian arm of the European Registry of mitral regurgitation, we compared the ability of GLS and LVEF to detect cardiac damage in patients with MR.

Methods: Five hundred four consecutive patients with MR underwent a complete echo-Doppler exam. A total of 431, 53 and 20 patients had degenerative, secondary and mixed MR, respectively. The main echocardiographic parameters, including LV and left atrial size measurements, pulmonary artery systolic pressure and GLS were compared between patients with mild MR (n = 392) vs. moderate to severe MR (n = 112).

Results: LVEF and GLS were related one another in the pooled population, and separately in patients with mild and moderate/severe MR (all $p < 0.0001$). However, a certain number of patients were above the upper or below the lower limits of the 95% confidence interval (CI) of the normal relation in the pooled population and in patients with mild MR. Only 2 patients were below the 95% CI in moderate to severe MR. After adjusting for confounders by separate multivariate models, LVEF and GLS were independently associated with LV and left atrial size in the pooled population and in mild and moderate/severe MR. GLS, but not LVEF, was also

independently associated with pulmonary artery systolic pressure in patients with mild and moderate to severe MR.

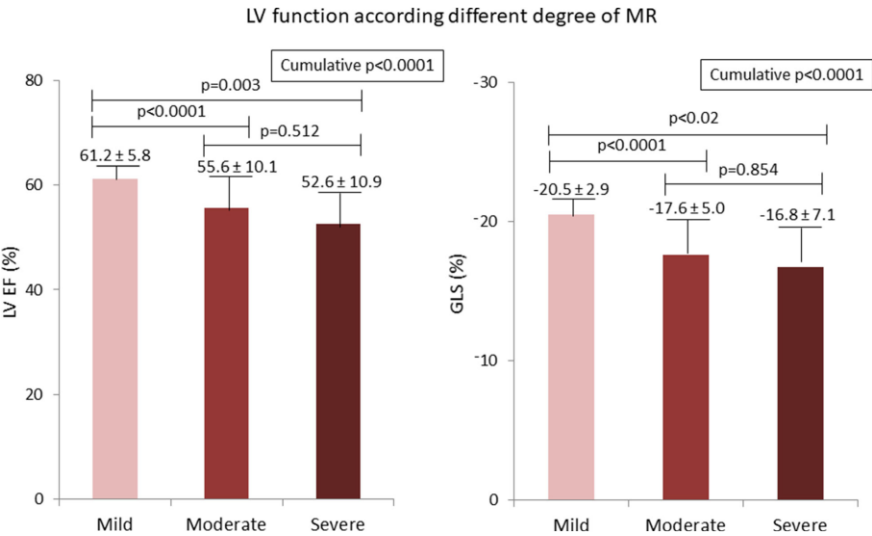


Figure 23. Differences in LVEF and GLS by MR degree.

Conclusions: Both LVEF and GLS are independently associated with LV and left atrial size, but only GLS is related to pulmonary arterial pressure. GLS is a powerful hallmark of cardiac damage in MR.

CHAPTER 16

Practical Impact of New Diastolic Recommendations on Non- invasive Estimation of Left Ventricular Diastolic Function and Filling Pressures

Background: In 2016⁶⁴, an update of the 2009⁶⁵ recommendations for the evaluation of LV diastolic function (DF) was released by the American Society of Echocardiography and the European Association of Cardiovascular Imaging. The aims of this study were to assess the concordance between the 2016 and 2009 recommendations and to test the impact of the consideration of “myocardial disease” recommended in the 2016 update on the evaluation of diastolic dysfunction and LV filling pressures in patients with normal and reduced LV ejection fractions referred to a general echocardiography laboratory.

Methods: A total of 1,508 outpatients referred to an echocardiography laboratory during a predefined 5-month period were prospectively enrolled. All patients underwent targeted clinical history and Doppler echocardiographic examination. Diastolic dysfunction and LV filling pressures were assessed according to 2009 and 2016 recommendations. Concordance was calculated using the k coefficient and overall proportion of agreement.

Results: Overall proportion of agreement between the two recommendations was 64.7% ($k = 0.43$). Comparing the 2009 and 2016 recommendations, 47.5% and 36.1% patients, respectively, had diastolic dysfunction ($P < 0.0001$), and 22.7% and 12.6% had elevated LV filling pressures ($P < 0.0001$). This difference remained significant in the setting of

patients with normal LV ejection fractions (21.6% vs 10.7%, $P < 0.0001$). In the application of the 2016 recommendations, whether or not the presence of “myocardial disease” was considered, the prevalence of indeterminate diastolic function was, respectively, 7.3% versus 13.7%, while patients in whom the diastolic disfunction grade could not be determined were 8.1% versus 14.4% ($P < 0.0001$ for all).

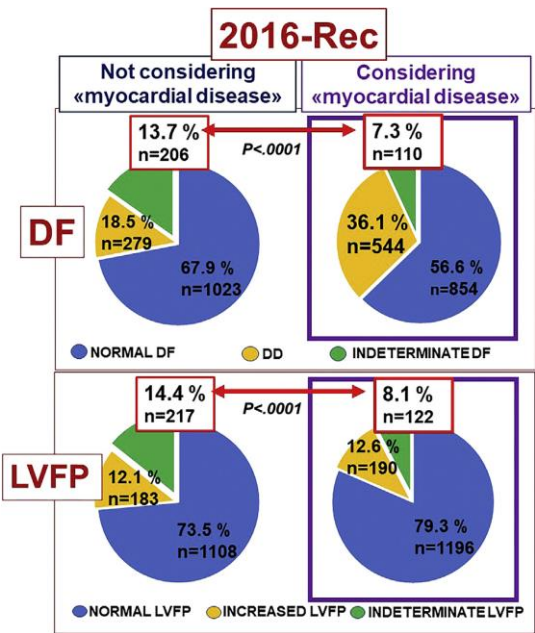


Figure 24. Application of the first-step work flow of the 2016 recommendations to all patients with normal LVEFs, considering or not considering the presence of “myocardial disease.” Comparison of estimates of DD and LVFP between the correct application of the 2016 recommendations (i.e., considering myocardial disease; left) versus 2016 recommendations applying the first step work flow to all patients with normal LVEFs (right, purple boxes). Not considering “myocardial disease” in the decision tree results in a significantly higher prevalence of patients with inconclusive diagnoses. Red arrows denote statistically significant differences of inconclusive diagnosis.

Conclusions: Considering the presence of myocardial disease when applying the 2016 recommendations resulted in a lower prevalence of inconclusive diagnosis.

Part III

Advanced imaging tools for evaluation of
fibrocalcific score in aortic valve stenosis:
the use of contrast-CT

CHAPTER 17

Contrast-enhanced computed tomography assessment of aortic stenosis

Background: Recent guidelines recommend non-contrast CT calcium scoring of the aortic valve (CT-AVC) as an arbiter of aortic stenosis severity when echocardiographic measurements are discordant¹³. This recommendation is based on data demonstrating the diagnostic accuracy of CT-AVC as a flow-independent measure and its correlation with disease progression and clinical events¹⁴⁻¹⁶. However, CT-AVC has several important limitations. First, it offers little detail about valve morphology and is unable to localise the anatomical distribution of calcium in the valve and surrounding structures. Second, CT-AVC cannot quantify fibrosis, an important contributor to valve stenosis, and may therefore misclassify disease severity, particularly in young females and those with bicuspid valves^{17, 18}. Thus, we assessed aortic valve calcific and non-calcific disease using contrast-enhanced CT.

Methods: This was a post hoc analysis of 164 patients [median age 71 (IQR 66–77) years, 78% male] with aortic stenosis (41 mild, 89 moderate, 34 severe; 7% bicuspid) who underwent echocardiography and contrast-enhanced CT as part of imaging studies. Calcific and non-calcific (fibrosis) valve tissue volumes were quantified and indexed to annulus area, using Hounsfield unit thresholds calibrated against blood pool radiodensity. The fibrocalcific ratio assessed the relative contributions of valve fibrosis and calcification. The fibrocalcific volume (sum of indexed non-calcific and calcific volumes) was compared with aortic valve peak velocity and, in a subgroup, histology and valve weight.

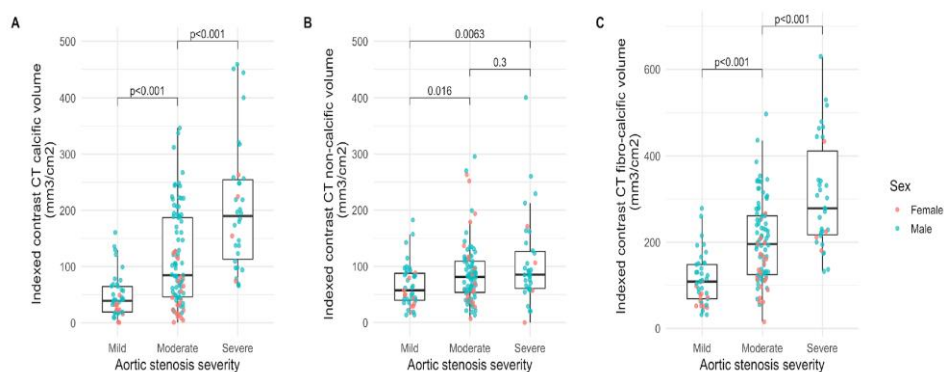


Figure 25. Indexed contrast CT leaflet volumes and aortic stenosis severity. Box plots of indexed contrast CT calcific (A), non-calcific (B), and fibrocalcific (C) volumes according to aortic stenosis severity. P values for Wilcoxon rank sum test.

	Peak aortic jet velocity	P value*
Agatston score†		
All	0.59	<0.001
Male	0.57	<0.001
Female	0.38	0.054
Indexed contrast CT fibrocalcific volume		
All	0.67	<0.001
Male	0.66	<0.001
Female	0.72	<0.001

*Spearman's rank correlation coefficients.

Table 9. Correlations between CT aortic valve assessments and echocardiography.

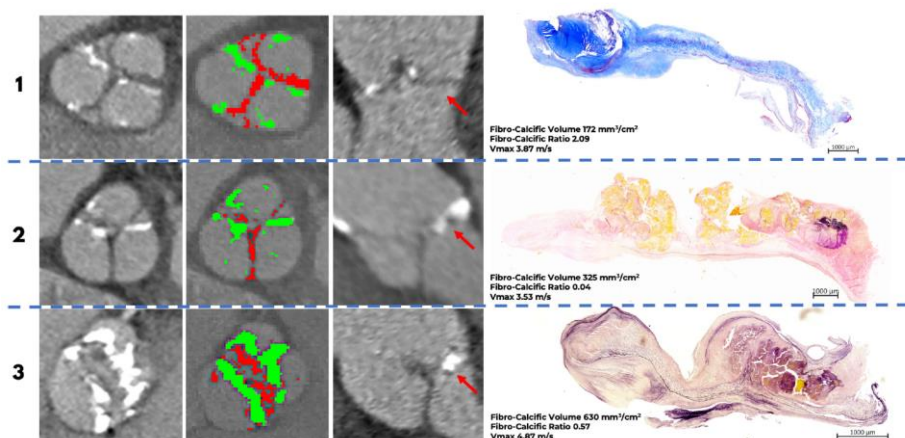


Figure 26. Contrast-enhanced CT and histology. Case 1: A tricuspid aortic valve from a woman with a large amount of fibrosis (red) compared with calcification (green) on CT. Histology confirms a preponderance of fibrosis in the valve consistent with the CT findings. There was no clear evidence of valve thrombosis or lipid infiltration. Red arrow denotes the leaflet corresponding to histology. Time from CT to surgery: 15 days. Masson's trichrome staining: blue sections represent collagen; red/purple represents calcium. Case 2: A tricuspid aortic valve from a man with a small amount of fibrosis compared with calcification (from the three CT slices containing the aortic valve this one was the only one with significant fibrosis). This was again confirmed on histological analysis of the valve leaflet. Red arrow denotes the leaflet corresponding to histology. Time from CT to surgery: 15 days. Verhoeff-van Gieson staining: black represents elastic fibres, pink collagen fibres and yellow calcium. Case 3: A bicuspid aortic valve from a man with extensive fibrosis and calcification in the valve. Findings were again confirmed on histology with the spatial distribution of calcium and fibrosis on histology appearing similar to the calcific and non-calcific leaflet thickening on CT (Verhoeff-van Gieson staining). Red arrow denotes the leaflet corresponding to histology. Time from CT to surgery: 21 days.

Results: Contrast-enhanced CT calcium volumes correlated with CT calcium score ($r=0.80$, $p<0.001$) and peak aortic jet velocity ($r=0.55$, $p<0.001$). The fibrocalcific ratio decreased with increasing aortic stenosis severity [mild: 1.29 (0.98–2.38), moderate: 0.87 (1.48–1.72), severe: 0.47 (0.33–0.78), $p<0.001$] while the fibrocalcific volume increased [mild: 109 (75–150), moderate: 191 (117–253), severe: 274 (213–344) mm³/cm²]. Fibrocalcific volume correlated with ex vivo valve weight ($r=0.72$, $p<0.001$). Compared

with the Agatston calcium score, fibrocalcific volume demonstrated a better correlation with peak aortic jet velocity ($r=0.59$ and $r=0.67$, respectively), particularly in females ($r=0.38$ and $r=0.72$, respectively).

Conclusions: Contrast-enhanced CT assessment of aortic valve calcific and non-calcific volumes correlates with aortic stenosis severity and may be preferable to non-contrast CT when fibrosis is a significant contributor to valve obstruction.

CHAPTER 18

Gaussian mixture model for evaluation of fibrocalcific score in aortic valve stenosis

Background: The evaluation of Agaston calcium score by non-contrast CT ignores the contribution of aortic valve fibrosis in aortic valve stenosis^{17, 18}. Fibrocalcific volume assessment by contrast-CT has been demonstrated to be an accurate method for the measure of aortic stenosis severity that quantifies both calcific and non-calcific leaflet volumes⁶⁶. However, currently used technologies for the computation of the fibrocalcific volume by contrast-CT are time-consuming and not easily applicable into clinical practice. We propose a new methodology for the assessment of the aortic valve fibro-calcific volume applying a gaussian mixture model for this aim.

Methods: A post-hoc analysis of a population including patients with aortic stenosis (from mild to severe) (n=136, males=107, females=29) undergoing contrast CT was performed. Once determined the aortic valve volume of interest, the software estimated the Hounsfield Units distribution of three populations (blood pool, non-calcific and calcific tissue) and thresholds for non-calcific (lower 99.7 percentile of blood pool HU) and calcific tissue (upper 99.7 percentile blood pool HU) were automatically generated. The time of analysis was less than 5 minutes for each scan. The obtained calcific and non-calcific volumes and the fibrocalcific volume were indexed for CT annulus area and compared with echocardiographic aortic valve peak velocity.

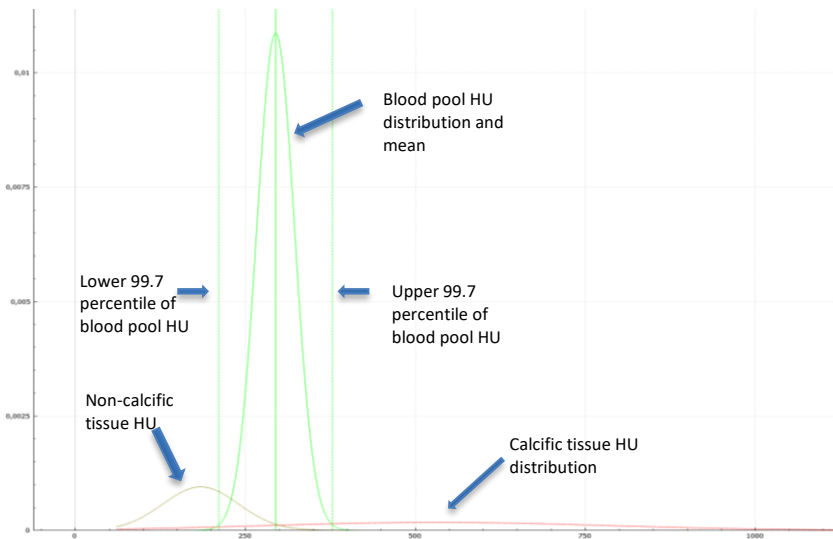
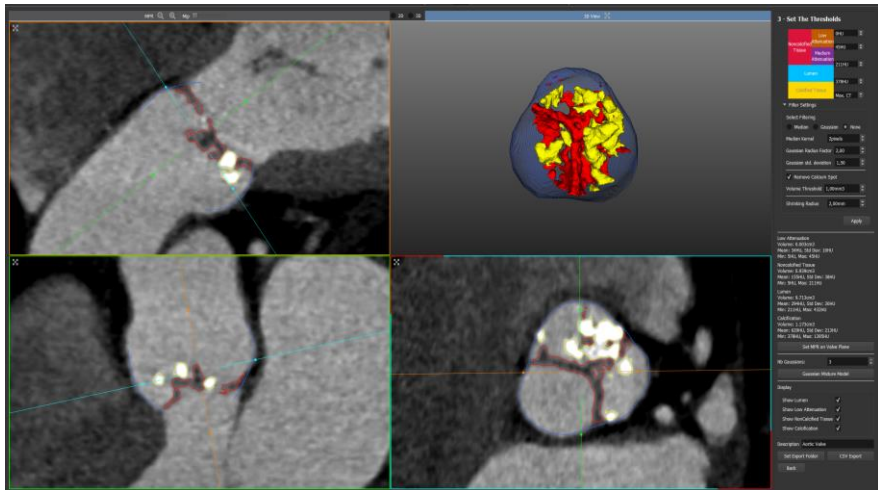


Figure 27. Upper panel: Assessment of Fibrocalcific volume by the Gaussian mixture model. Lower panel: Gaussian mixture model output showing the distribution of the three HU populations. According to this distribution thresholds for non-calcific (lower 99.7 percentile of blood pool HU) and calcific tissue (upper 99.7 percentile blood pool HU) were automatically generated.

Results: Intraobserver and interobserver reproducibility for the analysis of fibrocalcific volume by the Gaussian mixture model were excellent (both intraclass correlation coefficient =0.98). Fibrocalcific volume well correlated with echocardiographic aortic peak velocity ($\rho=0.70$, $p<0.0001$).

Considering sex distribution, despite similar correlation coefficient in males ($\rho=0.68$) and females ($\rho=0.71$) between fibrocalcific volume and aortic peak velocity, the correlation was mainly driven by the calcific volume in males whereas by non-calcific volume in females.

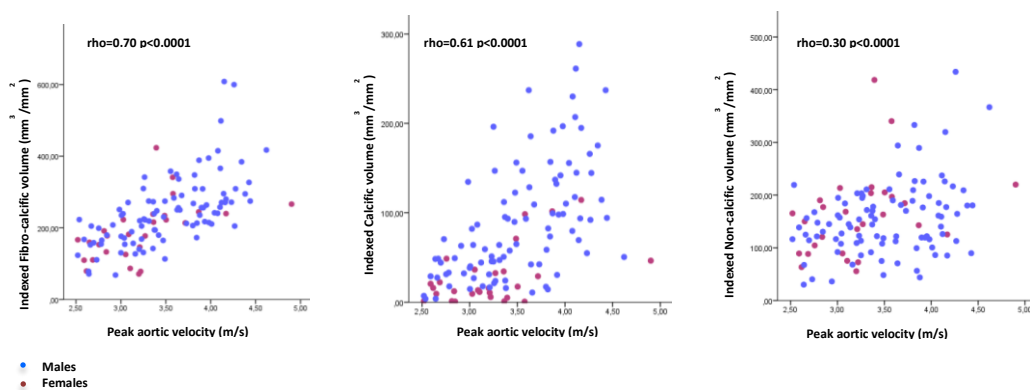


Figure 28. Scatterplots showing the correlations between the indexed fibrocalcific, calcific and non-calcific volume with echocardiographic aortic peak velocity.

Males n=107	Echo peak aortic velocity	Echo mean_gradient
Indexed_Non_calcific_volume	r=0.27 p<0.005	r=0.23 p<0.01
Indexed_Calcific_volume	r=0.59 p<0.0001	r=0.58 p<0.0001
Indexed_Fibrocalcific_volume	r=0.68 p<0.0001	r=0.64 p<0.0001
Females n=29	Echo peak aortic velocity	Echo mean_gradient
Indexed_Non_calcific_volume	r=0.47 p<0.01	r=0.49 p=0.008
Indexed_Calcific_volume	r=0.42 p<0.02	r=0.41 p=0.03
Indexed_Fibrocalcific_volume	r=0.71 p<0.0001	r=0.69 p<0.0001

Table 10. Correlations according to sex.

Conclusions: Gaussian mixture model application represents a valuable and reproducible way for the assessment of fibrocalcific volume in aortic valve stenosis, drastically reducing time for analysis. Further studies are needed for the derivation of fibrocalcific leaflet volume threshold for severe aortic stenosis.

Part IV

Advanced molecular imaging of thoracic aorta
by ^{18}F -Sodium Fluoride PET-CT for
identification of microcalcification activity
and stroke risk prediction

CHAPTER 19

Quantifying microcalcification activity in the thoracic aorta

Background: Standard methods for quantifying PET uptake in the aorta are time consuming and may not reflect overall vessel activity^{25, 26}. We describe aortic microcalcification activity (AMA), a novel method for quantifying 18F-NaF uptake in the thoracic aorta.

Methods: Twenty patients underwent two hybrid 18F-NaF PET and CT scans of the thoracic aorta less than three weeks apart. AMA, as well as maximum (TBRmax) and mean (TBRmean) tissue to background ratios, were calculated by two trained operators. Intra-observer repeatability, inter-observer repeatability and scan-rescan reproducibility were assessed. Each 18F-NaF quantification method was compared to validated cardiovascular risk scores.

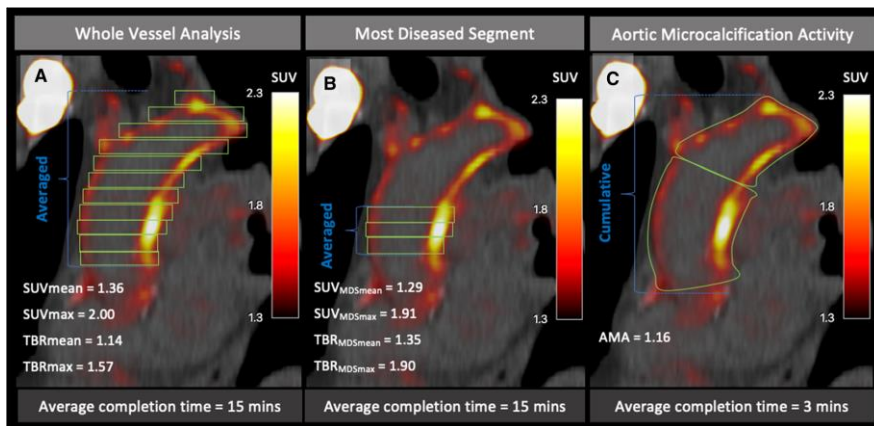


Figure 29. 18F-Sodium fluoride positron emission tomography and computed tomography in a patient with marked aortic wall uptake. An illustrated representation of standard whole vessel (A) and most diseased segment (B) as well as novel aortic microcalcification (C) methods for quantifying uptake. Average time taken to complete each method is shown. AMA, aortic microcalcification activity; Asc, ascending aorta; CT, computed tomography; PA, pulmonary artery; PET, positron emission tomography;

LV, left ventricle; RA, right atrium; TBR, tissue to background ratio.

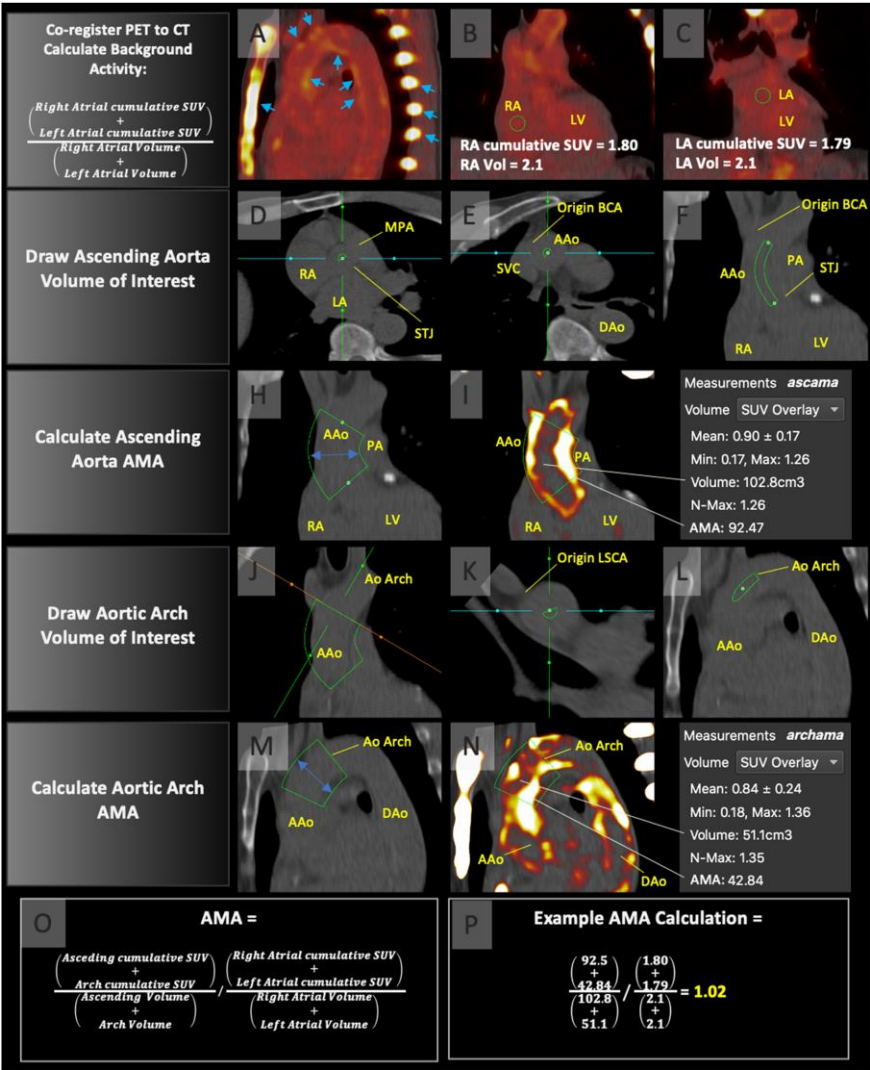


Figure 30. AMA step by step calculation.

Results: Aortic microcalcification activity demonstrated excellent intra-observer (intraclass correlation coefficient= 0.98) and inter-observer

(intraclass correlation coefficient= 0.97) repeatability with very good scan-rescan reproducibility (intraclass correlation coefficient 0.86) which were similar to previously described TBRmean and TBRmax methods. AMA analysis was much quicker to perform than standard TBR assessment (3.4min versus 15.1min, $P<0.0001$). AMA was correlated with Framingham stroke risk scores and Framingham risk score for hard coronary heart disease ($r=0.50$ and $r=0.44$ respectively, $p<0.05$).

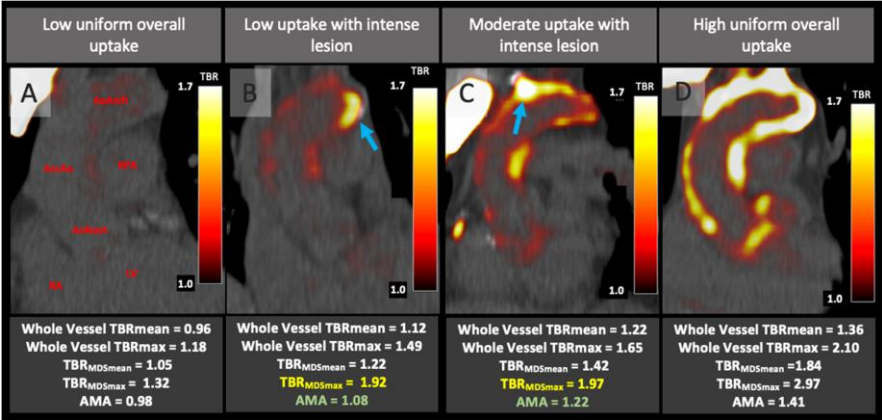


Figure 31. Hybrid 18F-sodium fluoride positron emission tomography and computed tomography coronal images of the ascending aorta and arch in four patients with varying patterns and intensity of aortic wall 18Fsodium fluoride activity: (A) Homogenously low activity across the ascending aorta and arch; (B) Generally low activity with a single high intensity lesion (blue arrow); (C) Moderate activity with a high intensity lesion (blue arrow); (D) High and intense activity throughout ascending aorta and arch. Note that (B) and (C) have similar values for most diseased segment maximum tissue to background ratio (highlighted in yellow) despite substantially different overall activity (aortic microcalcification activity values highlighted in green). AscAo, ascending aorta; AMA, aortic microcalcification activity; AoArch, aortic arch; AoRoot, aortic root; MDS, most diseased segment; LV, left ventricle; RA, right atrium; RPA, pulmonary artery; SUV, standardized uptake measurement; TBR, tissue to background ratio.

Conclusions: AMA is a simple, rapid and reproducible method of quantifying global 18FNaF uptake across the ascending aorta and aortic arch that correlates with cardiovascular risk scores.

CHAPTER 20

Thoracic Aortic 18F-Sodium Fluoride Activity and the Risk of Ischaemic Stroke in Patients with Established Cardiovascular Disease

Background: Aortic atherosclerosis represents an important contributor to ischaemic stroke risk⁶⁷. We investigated whether thoracic aortic atherosclerotic disease activity could improve the identification of patients at highest risk of ischaemic stroke.

Methods: In a post-hoc observational cohort study, we quantified thoracic aortic and coronary atherosclerotic disease activity in 461 patients with stable cardiovascular disease using thoracic 18F-sodium fluoride PET-CT. Progression of atherosclerosis was assessed by change in aortic and coronary CT calcium volume and clinical outcomes were determined by the occurrence of ischaemic stroke and myocardial infarction respectively. We compared the prognostic utility of atherosclerotic disease activity to clinical risk scores and CT calcium quantification using survival analysis and multivariable logistic regression.

Results: After 12.7 ± 2.7 months, progression of thoracic aortic calcium volume correlated with baseline aortic atherosclerotic disease activity ($n=140$, $r=0.31$, $p=0.00016$). In 461 patients, 23 (5%) patients experienced an ischaemic stroke and 32 (7%) myocardial infarction after 6.1 ± 2.3 years of follow up. High thoracic aortic atherosclerotic disease activity was strongly associated with ischaemic stroke [Hazard ratio 10.3 (3.1 to 34.8), $p=0.0017$], but not myocardial infarction ($p=0.40$). Conversely, high coronary

atherosclerotic disease activity was associated with myocardial infarction [Hazard ratio 4.8 (1.9 to 12.2), $p=0.00095$] but not ischaemic stroke ($p=0.39$). In a multivariable logistic regression model including imaging and clinical risk factors, thoracic aortic atherosclerotic disease activity was the only variable associated with ischaemic stroke [Odds ratio 1.76 (1.12 to 2.78), $p=0.0014$].

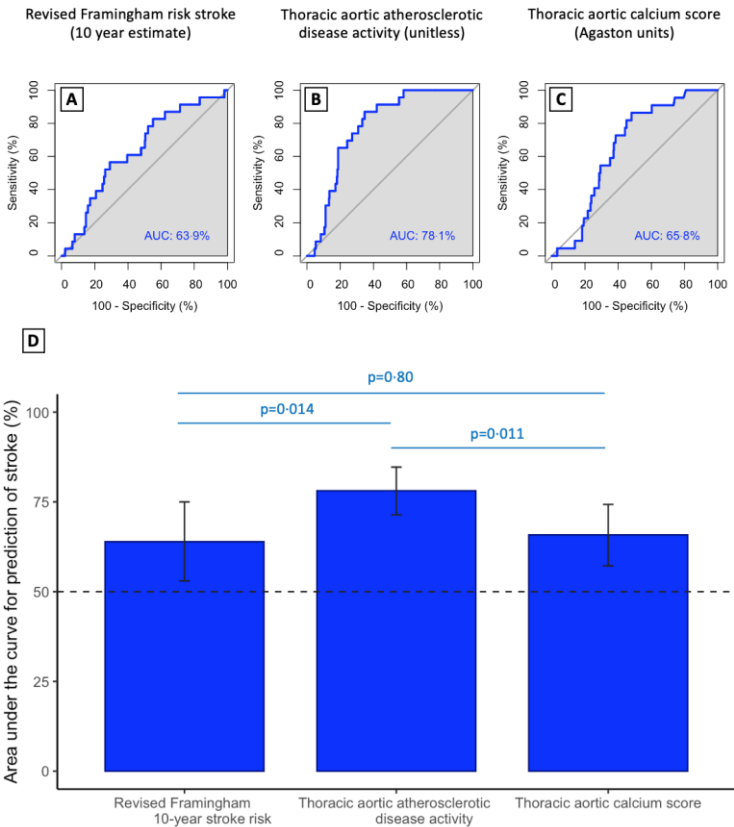
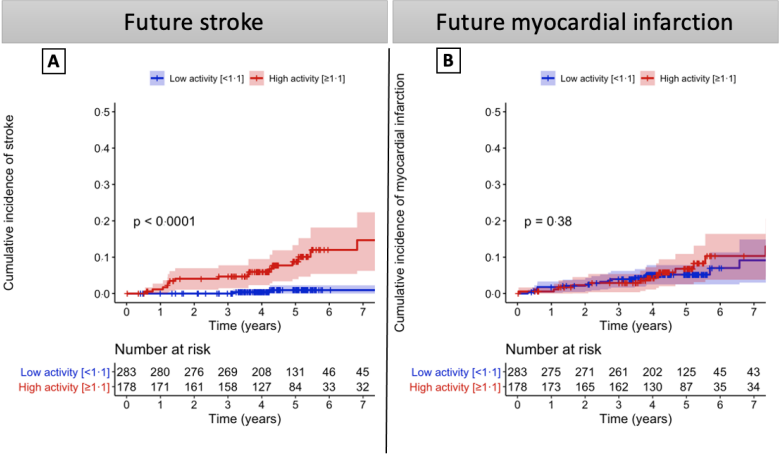


Figure 32. Area under the curve (AUC) for (A) 10-year stroke clinical risk score, (B) thoracic aortic atherosclerotic disease activity, and (C) thoracic aortic calcium score for the outcome of stroke. (D) Area under the curve analysis comparing thoracic aortic atherosclerotic disease activity, clinical risk score and thoracic aortic calcium score.

Thoracic aortic atherosclerotic activity



Coronary atherosclerotic activity

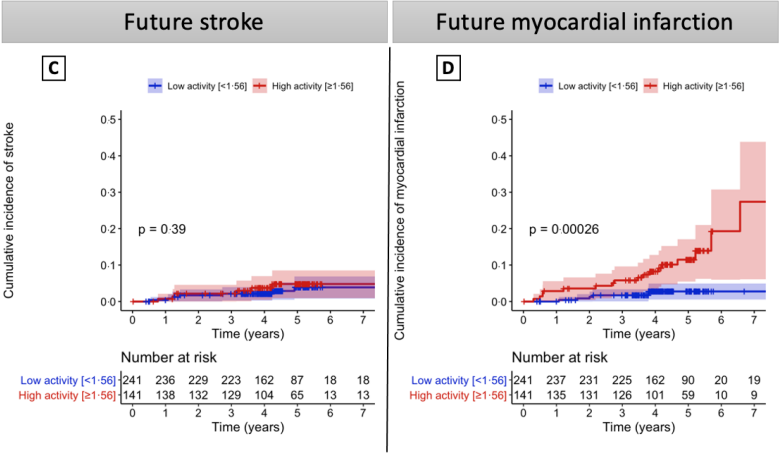


Figure 33. Cumulative incidence curves demonstrating freedom from stroke (A and C) or myocardial infarction (B and D) across the combined cohort. (A) Thoracic aortic atherosclerotic disease activity threshold of ≥ 1.1 (unitless) ($n=461$) is strongly associated with future stroke (hazard ratio 10.3 [3.1 to 34.8], $p=0.0017$), (B) but not myocardial infarction (hazard ratio 1.35 [0.67 to 2.7], $p=0.4$). (C) Coronary atherosclerotic disease activity ($n=382$, threshold 1.56) is not associated with future stroke (hazard ratio 1.59 [0.56 to 4.53] $p=0.39$) (D) but is strongly associated with future myocardial infarction (hazard ratio 4.8 [1.9 to 12.2], $p=0.0010$).

Conclusions: In patients with established cardiovascular disease, aortic

atherosclerotic disease activity predicts progression of calcific atherosclerosis in the thoracic aorta as well as the subsequent risk of ischemic stroke. Arterial ¹⁸F-sodium fluoride uptake identifies localized areas of atherosclerotic disease activity that are directly linked to disease progression and downstream regional clinical atherothrombotic events.

Part V

Discussion and conclusions

Discussion

Part I. Advanced cardiac ultrasound imaging for identification of early impairment in Hypertensive Heart Disease

Early identification of cardiac morphological and functional changes induced by arterial hypertension has become crucial for a timely and adequate treatment, aiming at not only the avoidance of irreparable organ damage but also for trying to confine injury progression, thus being relevant for defining patients' outcomes and prognosis⁶⁸. We have demonstrated that the use of advanced ultrasound imaging techniques, such as speckle tracking and 3D-echocardiography, are precious tools in this setting for the identification of early LV impairment.

Real-time 3D echocardiography allows the assessment of LV geometry and in particular the computation of LV mass and volumes, providing an accuracy that is comparable to MRI, the latter considered the gold standard for this evaluation¹⁰⁻¹². The use of LVM/EDV ratio, the so-called left ventricular remodelling index, already validated by MRI, has been proposed for the 3D-echocardiographic evaluation of left ventricular geometry in the hypertensive setting. Higher values of LVM/EDV ratio corresponded to the increase of left ventricular wall thickness in relation with left ventricular internal cavity size. Elevated values of LVM/EDV ratio by MRI were associated with more extended areas of left ventricular myocardial fibrosis and with poor prognosis in hypertensive patients^{28, 30}. In a population of newly diagnosed and never-treated hypertensive patients, using 3D-LVM/EDV ratio we were able to recognize a higher rate of hypertensive patients with left

ventricular concentric remodelling in comparison to 2D derived relative wall thickness; these patients also presented an impairment in stroke volume which is a reliable measure of LV pump performance, at least as important as, and perhaps more important than, LVEF. Hypertensive women, being more likely to develop left ventricular concentric remodelling in response to pressure overload, presented higher values of 3D-LVM/EDV ratio than men. In addition, in a subsequent study we also demonstrated that elevated 3D-LVM/EDV ratio identifies a cluster of native hypertensive patients with LV concentric geometry and subclinical LV diastolic and systolic dysfunction, 3D-LVM/EDV ratio being independently associated with both E/e' ratio and GLS. Accordingly, 3D-LVM/EDV ratio offers the possibility of identifying a group of hypertensive patients with LV diastolic and systolic dysfunction, and therefore more prone to development of overt heart failure, with a better accuracy than the traditionally used relative wall thickness, obtainable by 2D echo assessment. 3D-echocardiographic technique could represent a good compromise between 2D-echocardiography and MRI: it shows indeed advantages over standard 2D-echo, as it does not need geometrical assumptions and could overcome some limitations due to off-axis beam orientation and difficult evaluation of asymmetric LVH; it is also less expensive than MRI⁶⁹.

Furthermore, speckle tracking echocardiography is a simple and feasible technique and in particular GLS had the advantage to be able to detect an early systolic dysfunction, even before a drop in LVEF⁸. GLS was demonstrated to be altered even at early stages of arterial hypertension⁶. We evaluated longitudinal (by GLS) and circumferential (by MFS) systolic function and correlations between these two functional components in newly diagnosed hypertensive patients without clinically defined LVH. LV systole is

the result of simultaneous contraction of myocardial fibers, which are differently arranged in three – subendocardial, midwall and subepicardial – layers. Myocardial fibers, aligned longitudinally in subendocardial and subepicardial layers and circumferentially in the midwall one, contribute to global LV mechanics, including reduction of minor axis, shortening of long axis and apical twisting^{70, 71}. Myocardial layers are intimately connected in multiple directions with a gradual transition among different orientations, creating a helicoidal LV architecture⁷². Both GLS and MFS express intrinsic LV wall mechanics on different planes. MFS reflects a regional shortening corrected for end-diastolic and end-systolic length³⁵. GLS expresses the shortening of longitudinally oriented cardiomyocytes in subendocardium and subepicardium³. We demonstrated that first, despite normal ejection fraction, newly diagnosed and never-treated hypertensive patients without clinically defined LVH had lower GLS and MFS than healthy normotensive controls; second, hypertensive patients with abnormal GLS showed also an impairment of midwall circumferential fibers, that is a lower MFS; third, MFS was positively associated with GLS independently on several confounders; fourth, the association between MFS and GLS remained significant even in hypertensive patients with normal LV geometry.

Regional LS analysis provided further information. Previous experiences already reported that lower basal LS than apical LS and an exacerbation of base-to-apex LS gradient might be evident also in hypertensive patients with concentric LVH^{73, 74}. This parallels myocardial fibrosis that is found predominantly in LV basal and middle segments of hypertensive concentric LVH by late gadolinium enhancement cardiac MRI⁷⁵. We extended these findings to early stage of hypertensive disease without clear-cut LVH, demonstrating that despite normal LV EF, LS dysfunction is detectable in

hypertensive patients, mainly involving basal and middle segments, resulting in higher relative regional strain ratio.

We also evaluated that lower values of MEEi, an echo-derived parameter of LV performance⁷⁶, at baseline identified hypertensive patients more liable to develop LVEF reduction. Thus, the use of MEEi could be helpful to define the risk profile of hypertensive patients and could represent an important parameter for predicting future development of LV systolic dysfunction in this setting.

All these findings demonstrated that the combination of standard and advanced echocardiographic techniques should be carefully considered to diagnose subclinical cardiac organ damage in hypertensive heart disease, stratify prognosis and address patients' management. Since different imaging tools could provide complementary information, a multi-imaging approach thus may help to have a more exhaustive perspective of arterial hypertension induced cardiovascular damage.

Part II. Advanced ultrasound cardiac imaging in other cardiovascular diseases

Advanced ultrasound imaging tools are extremely useful for the evaluation of cardiac function in several different clinical settings and diseases in which a cardiac involvement can occur. These techniques can help in the identification of subclinical cardiovascular impairment and in properly and timely addressing patients' care. Speckle tracking derived GLS is a sensible echo parameter for detection of an early LV dysfunction.

We applied the GLS strategy suggested by the ASE/EACVI Expert Consensus

to identify subclinical CTRCD⁴⁶ and timely started cardioprotection. The superior feasibility⁷⁷ and reproducibility (inter-exam variability of about 6%) of GLS in comparison with EF (about 10%) makes this parameter suitable for monitoring systolic function during chemotherapy. A GLS drop >15% from baseline is a concrete variation to predict heart failure in cancer patients undergoing concurrent trastuzumab and anthracycline therapy, independently on baseline LVEF⁴⁶. We demonstrated that in a population of HER2-positive breast cancer patients undergoing adjuvant therapy: (i) the use of GLS allows to identify subclinical CTRCD when LVEF is still normal; (ii) all the patients developing subclinical CTRCD without progression towards overt heart failure were able to complete CT without interruption, thanks to cardioprotective treatment; (iii) among the four patients developing subsequent overt CTRCD, three could complete CT with an adequate cardioprotective treatment; (iv) in the subgroup of patients without CTRCD a reduction in LVEF and GLS and an increase in E/e' ratio was detected at the end of CT in comparison with baseline.

In addition, we demonstrated that GLS and regional LS evaluations are able to identify an early LV systolic impairment in patients affected by AFD. In naive AFD patients, we observed an early reduction of LV LS, involving mainly LV basal myocardial segments with an exacerbation of the base-to-apex longitudinal gradient deformation and resulting in an increase in regional strain ratio. Nevertheless, the association found between the higher lysoGB3 levels and the lower apical cap LS demonstrates that apical segments LS, despite still normal, is not spared at diagnosis.

GLS was demonstrated to be a sensitive parameter even for the evaluation of LV systolic progressive impairment in patients with MR.

Moreover, we investigated the evidence of LV dysfunction in APS, a multisystemic autoimmune disease, and we demonstrated that, in APS patients without CAD and hemodynamically significant valve heart disease, abnormalities of LV diastolic function involve not only LV filling (transmitral E/A ratio) but also myocardial relaxation (e' velocity) and E/ e' ratio; LV diastolic abnormalities were more severe in primary than in secondary APS and in the pooled APS population, average e' velocity was independently associated with the lupus anticoagulant positivity.

In addition, in the evaluation of LV diastolic function according to current guidelines in a wide population examining outpatients affected by multiple diseases, we emphasized that considering the presence of myocardial disease when applying the 2016 recommendations for LV diastolic function resulted in a lower prevalence of inconclusive diagnosis.

Furthermore, the application of speckle tracking echocardiography and 3D-assessment to the right ventricle could provide valuable information in particular clinical settings. We investigated LV and RV echocardiographic features of IPF and no-IPF patients without evidence of any other heart disease, in relation with a healthy control group. In this setting we demonstrated that a clear alteration of RV geometry and of both systolic (in RV EF by 3D-echo and GLS) and diastolic function, and a substantial pulmonary arterial systolic pressure increase in comparison with controls, whereas no-IPF patients present only an alteration of RV diastolic dysfunction and a lower degree of pulmonary arterial systolic pressure increase. Moreover, an independent association between DLCOsb and RV longitudinal dysfunction is found in the pooled population affected by interstitial lung disease, it being evident in the IPF group but not the no-IPF group.

All these findings corroborated the usefulness of advanced ultrasound tools for the evaluation of cardiac early impairment in multiple different settings.

Part III. Advanced imaging tools for evaluation of fibrocalcific score in aortic valve stenosis: the use of contrast-CT

We evaluated a novel method of contrast-enhanced CT analysis that allows assessment of both aortic valve calcification and non-calcific leaflet thickening (fibrosis) in patients with aortic valve stenosis. We demonstrated the feasibility of contrast-enhanced CT assessment of aortic stenosis severity, with the indexed fibrocalcific volume correlating better with peak aortic jet velocity than CT-AVC in this cohort, particularly in females. Quantifying valve fibrosis, an aspect of valvular disease that cannot be assessed with non-contrast CT, may be therefore important in particular settings. Given the routine use of contrast-enhanced CT in clinical workflows for transcatheter aortic valve implantation, fibrocalcific volumes could be readily integrated into clinical practice, providing an alternative assessment for patients with uncertain disease severity. Discordant echocardiographic measures of aortic stenosis severity are observed in around one-third of patients^{14, 78}. CT-AVC has emerged as a useful tool in these patients, providing an anatomical, flow-independent assessment of disease severity that is well validated in concordant disease and supported by international guidelines. We found that assessments of valve calcification on contrast-enhanced CT correlated well with CT-AVC. However, progressive valve stiffening and narrowing in aortic stenosis occurs due to both fibrosis and calcification,^{79, 80} and CT-AVC, which quantifies only the latter, may underestimate aortic stenosis severity

in cases where valve obstruction is predominantly due to the former. We found the fibrocalcific volume to be a good measure of aortic stenosis severity that correlated well with echocardiographic measurements of valve haemodynamics and compared favorably with CT-AVC. Contrast-enhanced CT leaflet volumes also correlated with valve weight and semiquantitative histological assessments of calcification and fibrosis. The novel image analysis protocol proposed the use of flexible thresholds for defining calcific and non-calcific valve thickening based on contrast attenuation in the blood pool, and defined the aortic valve plane and annulus sizing in a uniform fashion that is well established, but had the disadvantage to be very time-consuming (about 45 minutes for each scan).

Thus, we also proposed the introduction of a Gaussian mixture model as an innovative approach to contrast-CT for the evaluation of fibrocalcific volume in aortic valve stenosis, sensibly reducing the time for analysis and obtaining excellent intra and inter observer reproducibility and optimal correlation between valve fibrocalcific volume and echocardiographic aortic peak velocity. Considering sex distribution, despite similar correlation coefficient in males and females between fibrocalcific volume and aortic peak velocity, the correlation was mainly driven by the calcific volume in males whereas by non-calcific volume in females, corroborating previous evidence showing lower valve calcium load in females, even indexed for body size. Thus, the aortic valve fibrocalcific volume as assessed by contrast-enhanced CT is an accurate and reproducible measure of aortic stenosis severity that quantifies both calcific and non-calcific leaflet volumes.

**Part IV. Advanced molecular imaging of thoracic aorta by
18F-Sodium Fluoride PET-CT for identification of microcalcification activity
and stroke risk prediction.**

Molecular imaging techniques are increasingly being used for investigating disease activity in the cardiovascular system^{25, 26}. We describe a novel method, AMA, which quantifies 18F-NaF across both the ascending aorta and aortic arch, providing a measure of overall burden of disease activity in these vessels. We demonstrate this method as being highly reproducible and more time efficient than the whole vessel technique. Moreover, it can be performed with a non-contrast CT, and does not require advanced post-processing techniques, such as motion or time-delay correction, making it potentially more widely applicable. Out of all methods assessed including TBR max, TBR mean and whole vessel analysis, AMA had the strongest correlation with Framingham stroke risk score.

In addition, we applied AMA assessment together with the evaluation of coronary microcalcification activity by PET-CT in a population with established cardiovascular disease. We were able to demonstrate that thoracic aortic atherosclerotic disease activity was associated with both progression of aortic atherosclerosis and subsequent 10-fold risk of ischaemic stroke. Moreover, we observed that atherosclerotic 18F-NaF uptake was specific to the circulation being assessed, with coronary atherosclerotic disease activity being able to identify those at risk of myocardial infarction but not stroke, whereas thoracic aortic atherosclerotic disease activity identified ischaemic stroke risk but not the risk of myocardial infarction.

Conclusions

During this research journey we investigated: a) the role of advanced ultrasound imaging tools, as speckle tracking and 3D- echocardiography, for the evaluation of early cardiac damage in hypertensive heart disease; b) the role of advanced ultrasound techniques in detecting subclinical cardiac impairment in multiple different diseases, including AFD, APS, CTRCD, interstitial lung diseases; c) the accuracy and feasibility of contrast-CT for the innovative evaluation of fibrocalcific volume in aortic valve stenosis; d) the use of advanced molecular imaging of thoracic aorta by 18F-Sodium Fluoride PET-CT for identification of microcalcification activity and ischemic stroke risk prediction.

The use of advanced imaging tools, representing the common denominator of this research, reflects the capability of different techniques in supplying precious information about morphological and functional cardiac impairment in multiple different settings, also providing valuable parameters for assessing better risk stratification and appropriately and timely addressing patients' management.

List of abbreviations

2D = two-dimensional

3D = three-dimensional

$^{18}\text{F-NaF}$ = ^{18}F -sodium fluoride

AFD = Anderson-Fabry disease

aGAPSS = adjusted global antiphospholipid syndrome score

ALS = apical longitudinal strain

AMA= aortic microcalcification activity

APS = Antiphospholipid syndrome

BLS = basal longitudinal strain

CAD= coronary artery disease

CPET = Cardiopulmonary exercise test

CT = computed tomography

CT-AVC = non-contrast CT calcium scoring of the aortic valve

CTRCD = Cancer therapy-related cardiac dysfunction

DF = diastolic function

DLCOSb = diffusion capacity for carbon monoxide

EDV = end-diastolic volume

GLS = global longitudinal strain

IPF = idiopathic pulmonary fibrosis

LS = longitudinal strain

LV = left ventricular

LVEF = left ventricular ejection fraction

LVH = left ventricular hypertrophy

LVM = left ventricular mass

LVM/EDV =left ventricular mass/end-diastolic volume ratio

MFS = Midwall fractional shortening

MLS= middle longitudinal strain

MEEi= indexed mechano-energetic efficiency

MR= mitral regurgitation

MRI = magnetic resonance imaging

PET= positron emission tomography

PET-CT = positron emission tomography -computed tomography

RV = right ventricular

RVEF= right ventricular ejection fraction

TBR= tissue to background ratio

Bibliography

1. Di Carli MF, Geva T, Davidoff R. The Future of Cardiovascular Imaging. *Circulation* 2016;**133**(25):2640-61.
2. Cameli M, Lembo M, Sciaccaluga C, Bandera F, Ciccone MM, D'Andrea A, D'Ascenzi F, Esposito R, Evola V, Liga R, Mandoli GE, Palmiero P, Santoro C, Scicchitano P, Sorrentino R, Zito A, Pedrinelli R, Mondillo S, Mattioli AV, Galderisi M, Working Groups of E, Arterial Hypertension of Italian Society of C. Identification of cardiac organ damage in arterial hypertension: insights by echocardiography for a comprehensive assessment. *J Hypertens* 2020;**38**(4):588-598.
3. Mor-Avi V, Lang RM, Badano LP, Belohlavek M, Cardim NM, Derumeaux G, Galderisi M, Marwick T, Nagueh SF, Sengupta PP, Sicari R, Smiseth OA, Smulevitz B, Takeuchi M, Thomas JD, Vannan M, Voigt JU, Zamorano JL. Current and evolving echocardiographic techniques for the quantitative evaluation of cardiac mechanics: ASE/EAE consensus statement on methodology and indications endorsed by the Japanese Society of Echocardiography. *Eur J Echocardiogr* 2011;**12**(3):167-205.
4. Mondillo S, Galderisi M, Mele D, Cameli M, Lomoriello VS, Zaca V, Ballo P, D'Andrea A, Muraru D, Losi M, Agricola E, D'Errico A, Buralli S, Sciomer S, Nistri S, Badano L, Echocardiography Study Group Of The Italian Society Of C. Speckle-tracking echocardiography: a new technique for assessing myocardial function. *J Ultrasound Med* 2011;**30**(1):71-83.
5. Geyer H, Caracciolo G, Abe H, Wilansky S, Carerj S, Gentile F, Nesser HJ, Khandheria B, Narula J, Sengupta PP. Assessment of myocardial mechanics using speckle tracking echocardiography: fundamentals and clinical applications. *J Am Soc Echocardiogr* 2010;**23**(4):351-69; quiz 453-5.
6. Lembo M, Esposito R, Lo Iudice F, Santoro C, Izzo R, De Luca N, Trimarco B, de Simone G, Galderisi M. Impact of pulse pressure on left ventricular global longitudinal strain in normotensive and newly diagnosed, untreated hypertensive patients. *J Hypertens* 2016;**34**(6):1201-7.
7. Farsalinos KE, Daraban AM, Unlu S, Thomas JD, Badano LP, Voigt JU. Head-to-Head Comparison of Global Longitudinal Strain Measurements among Nine Different Vendors: The EACVI/ASE Inter-Vendor Comparison Study. *J Am Soc Echocardiogr* 2015;**28**(10):1171-1181, e2.
8. Galderisi M, Trimarco B. Global longitudinal strain: a novel hallmark of cardiac risk in arterial hypertension. *J Hypertens* 2016;**34**(6):1050-1.
9. Contaldi C, Imbriaco M, Alcidi G, Ponsiglione A, Santoro C, Puglia M, Barbuto L, Cuocolo A, Trimarco B, Galderisi M. Assessment of the relationships between left ventricular filling pressures and longitudinal

dysfunction with myocardial fibrosis in uncomplicated hypertensive patients. *Int J Cardiol* 2016;**202**:84-6.

10. Yap SC, van Geuns RJ, Nemes A, Meijboom FJ, McGhie JS, Geleijnse ML, Simoons ML, Roos-Hesselink JW. Rapid and accurate measurement of LV mass by biplane real-time 3D echocardiography in patients with concentric LV hypertrophy: comparison to CMR. *Eur J Echocardiogr* 2008;**9**(2):255-60.

11. Pouleur AC, le Polain de Waroux JB, Pasquet A, Gerber BL, Gerard O, Allain P, Vanoverschelde JL. Assessment of left ventricular mass and volumes by three-dimensional echocardiography in patients with or without wall motion abnormalities: comparison against cine magnetic resonance imaging. *Heart* 2008;**94**(8):1050-7.

12. Mor-Avi V, Sugeng L, Weinert L, MacEneaney P, Caiani EG, Koch R, Salgo IS, Lang RM. Fast measurement of left ventricular mass with real-time three-dimensional echocardiography: comparison with magnetic resonance imaging. *Circulation* 2004;**110**(13):1814-8.

13. Baumgartner H, Falk V, Bax JJ, De Bonis M, Hamm C, Holm PJ, Iung B, Lancellotti P, Lansac E, Rodriguez Munoz D, Rosenhek R, Sjogren J, Tornos Mas P, Vahanian A, Walther T, Wendler O, Windecker S, Zamorano JL, Group ESCSD. 2017 ESC/EACTS Guidelines for the management of valvular heart disease. *Eur Heart J* 2017;**38**(36):2739-2791.

14. Clavel MA, Messika-Zeitoun D, Pibarot P, Aggarwal SR, Malouf J, Araoz PA, Michelena HI, Cueff C, Larose E, Capoulade R, Vahanian A, Enriquez-Sarano M. The complex nature of discordant severe calcified aortic valve disease grading: new insights from combined Doppler echocardiographic and computed tomographic study. *J Am Coll Cardiol* 2013;**62**(24):2329-38.

15. Clavel MA, Pibarot P, Messika-Zeitoun D, Capoulade R, Malouf J, Aggarwal S, Araoz PA, Michelena HI, Cueff C, Larose E, Miller JD, Vahanian A, Enriquez-Sarano M. Impact of aortic valve calcification, as measured by MDCT, on survival in patients with aortic stenosis: results of an international registry study. *J Am Coll Cardiol* 2014;**64**(12):1202-13.

16. Pawade T, Clavel MA, Tribouilloy C, Dreyfus J, Mathieu T, Tastet L, Renard C, Gun M, Jenkins WSA, Macron L, Sechrist JW, Lacomis JM, Nguyen V, Galian Gay L, Cuellar Calabria H, Ntalas I, Cartlidge TRG, Prendergast B, Rajani R, Evangelista A, Cavalcante JL, Newby DE, Pibarot P, Messika Zeitoun D, Dweck MR. Computed Tomography Aortic Valve Calcium Scoring in Patients With Aortic Stenosis. *Circ Cardiovasc Imaging* 2018;**11**(3):e007146.

17. Shen M, Tastet L, Capoulade R, Larose E, Bedard E, Arsenault M, Chetaille P, Dumesnil JG, Mathieu P, Clavel MA, Pibarot P. Effect of age and aortic valve anatomy on calcification and haemodynamic severity of aortic stenosis. *Heart* 2017;**103**(1):32-39.

18. Simard L, Cote N, Dagenais F, Mathieu P, Couture C, Trahan S, Bosse Y, Mohammadi S, Page S, Joubert P, Clavel MA. Sex-Related Discordance Between Aortic Valve Calcification and Hemodynamic Severity of Aortic Stenosis: Is Valvular Fibrosis the Explanation? *Circ Res* 2017;**120**(4):681-691.
19. Dweck MR, Williams MC, Moss AJ, Newby DE, Fayad ZA. Computed Tomography and Cardiac Magnetic Resonance in Ischemic Heart Disease. *J Am Coll Cardiol* 2016;**68**(20):2201-2216.
20. Achenbach S, Delgado V, Hausleiter J, Schoenhagen P, Min JK, Leipsic JA. SCCT expert consensus document on computed tomography imaging before transcatheter aortic valve implantation (TAVI)/transcatheter aortic valve replacement (TAVR). *J Cardiovasc Comput Tomogr* 2012;**6**(6):366-80.
21. Blanke P, Weir-McCall JR, Achenbach S, Delgado V, Hausleiter J, Jilaihawi H, Marwan M, Norgaard BL, Piazza N, Schoenhagen P, Leipsic JA. Computed Tomography Imaging in the Context of Transcatheter Aortic Valve Implantation (TAVI)/Transcatheter Aortic Valve Replacement (TAVR): An Expert Consensus Document of the Society of Cardiovascular Computed Tomography. *JACC Cardiovasc Imaging* 2019;**12**(1):1-24.
22. Irkle A, Vesey AT, Lewis DY, Skepper JN, Bird JL, Dweck MR, Joshi FR, Gallagher FA, Warburton EA, Bennett MR, Brindle KM, Newby DE, Rudd JH, Davenport AP. Identifying active vascular microcalcification by (18)F-sodium fluoride positron emission tomography. *Nat Commun* 2015;**6**:7495.
23. Dweck MR, Chow MW, Joshi NV, Williams MC, Jones C, Fletcher AM, Richardson H, White A, McKillop G, van Beek EJ, Boon NA, Rudd JH, Newby DE. Coronary arterial 18F-sodium fluoride uptake: a novel marker of plaque biology. *J Am Coll Cardiol* 2012;**59**(17):1539-48.
24. Kwiecinski J, Tzolos E, Adamson PD, Cadet S, Moss AJ, Joshi N, Williams MC, van Beek EJR, Dey D, Berman DS, Newby DE, Slomka PJ, Dweck MR. Coronary (18)F-Sodium Fluoride Uptake Predicts Outcomes in Patients With Coronary Artery Disease. *J Am Coll Cardiol* 2020;**75**(24):3061-3074.
25. Blomberg BA, de Jong PA, Thomassen A, Lam MGE, Vach W, Olsen MH, Mali W, Narula J, Alavi A, Hoilund-Carlsen PF. Thoracic aorta calcification but not inflammation is associated with increased cardiovascular disease risk: results of the CAMONA study. *Eur J Nucl Med Mol Imaging* 2017;**44**(2):249-258.
26. Blomberg BA, Thomassen A, de Jong PA, Simonsen JA, Lam MG, Nielsen AL, Mickley H, Mali WP, Alavi A, Hoilund-Carlsen PF. Impact of Personal Characteristics and Technical Factors on Quantification of Sodium 18F-Fluoride Uptake in Human Arteries: Prospective Evaluation of Healthy Subjects. *J Nucl Med* 2015;**56**(10):1534-40.
27. Schumann CL, Jaeger NR, Kramer CM. Recent Advances in Imaging of Hypertensive Heart Disease. *Curr Hypertens Rep* 2019;**21**(1):3.

28. Rodrigues JC, Amadu AM, Dastidar AG, Szantho GV, Lyen SM, Godsavage C, Ratcliffe LE, Burchell AE, Hart EC, Hamilton MC, Nightingale AK, Paton JF, Manghat NE, Bucciarelli-Ducci C. Comprehensive characterisation of hypertensive heart disease left ventricular phenotypes. *Heart* 2016;**102**(20):1671-9.
29. Siddiqui MA, Mittal PK, Little BP, Miller FH, Akduman EI, Ali K, Sartaj S, Moreno CC. Secondary Hypertension and Complications: Diagnosis and Role of Imaging. *Radiographics* 2019;**39**(4):1036-1055.
30. Heckbert SR, Post W, Pearson GD, Arnett DK, Gomes AS, Jerosch-Herold M, Hundley WG, Lima JA, Bluemke DA. Traditional cardiovascular risk factors in relation to left ventricular mass, volume, and systolic function by cardiac magnetic resonance imaging: the Multiethnic Study of Atherosclerosis. *J Am Coll Cardiol* 2006;**48**(11):2285-92.
31. Koitabashi N, Kass DA. Reverse remodeling in heart failure--mechanisms and therapeutic opportunities. *Nat Rev Cardiol* 2011;**9**(3):147-57.
32. Goldstein S, Sabbah H. Ventricular remodeling and angiotensin-converting enzyme inhibitors. *J Cardiovasc Pharmacol* 1994;**24 Suppl 3**:S27-31.
33. Galderisi M, Esposito R, Schiano-Lomoriello V, Santoro A, Ippolito R, Schiattarella P, Strazzullo P, de Simone G. Correlates of global area strain in native hypertensive patients: a three-dimensional speckle-tracking echocardiography study. *Eur Heart J Cardiovasc Imaging* 2012;**13**(9):730-8.
34. Streeter DD, Jr., Spotnitz HM, Patel DP, Ross J, Jr., Sonnenblick EH. Fiber orientation in the canine left ventricle during diastole and systole. *Circ Res* 1969;**24**(3):339-47.
35. de Simone G, Devereux RB, Roman MJ, Ganau A, Saba PS, Alderman MH, Laragh JH. Assessment of left ventricular function by the midwall fractional shortening/end-systolic stress relation in human hypertension. *J Am Coll Cardiol* 1994;**23**(6):1444-51.
36. Williams B, Mancia G, Spiering W, Agabiti Rosei E, Azizi M, Burnier M, Clement DL, Coca A, de Simone G, Dominiczak A, Kahan T, Mahfoud F, Redon J, Ruilope L, Zanchetti A, Kerins M, Kjeldsen SE, Kreutz R, Laurent S, Lip GYH, McManus R, Narkiewicz K, Ruschitzka F, Schmieder RE, Shlyakhto E, Tsioufis C, Aboyans V, Desormais I, Group ESCSD. 2018 ESC/ESH Guidelines for the management of arterial hypertension. *Eur Heart J* 2018;**39**(33):3021-3104.
37. Galderisi M, Cosyns B, Edvardsen T, Cardim N, Delgado V, Di Salvo G, Donal E, Sade LE, Ernande L, Garbi M, Grapsa J, Hagendorff A, Kamp O, Magne J, Santoro C, Stefanidis A, Lancellotti P, Popescu B, Habib G, Committee ESD, Committee ESD. Standardization of adult transthoracic echocardiography reporting in agreement with recent chamber quantification, diastolic

function, and heart valve disease recommendations: an expert consensus document of the European Association of Cardiovascular Imaging. *Eur Heart J Cardiovasc Imaging* 2017;**18**(12):1301-1310.

38. Mondillo S, Cameli M, Caputo ML, Lisi M, Palmerini E, Padeletti M, Ballo P. Early detection of left atrial strain abnormalities by speckle-tracking in hypertensive and diabetic patients with normal left atrial size. *J Am Soc Echocardiogr* 2011;**24**(8):898-908.

39. Dini FL, Galderisi M, Nistri S, Buralli S, Ballo P, Mele D, Badano LP, Faggiano P, de Gregorio C, Rosa GM, Ciavarella M, De Marco E, Borruso E, Marti G, Mondillo S, Marino PN, Cardiology SHCotWGoEotIso. Abnormal left ventricular longitudinal function assessed by echocardiographic and tissue Doppler imaging is a powerful predictor of diastolic dysfunction in hypertensive patients: the SPHERE study. *Int J Cardiol* 2013;**168**(4):3351-8.

40. Milan A, Tosello F, Naso D, Avenatti E, Leone D, Magnino C, Veglio F. Ascending aortic dilatation, arterial stiffness and cardiac organ damage in essential hypertension. *J Hypertens* 2013;**31**(1):109-16.

41. Katsi V, Georgiopoulos G, Oikonomou D, Aggeli C, Grassos C, Papadopoulos DP, Thomopoulos C, Marketou M, Dimitriadis K, Toutouzas K, Nihoyannopoulos P, Tsioufis C, Tousoulis D. Aortic Stenosis, Aortic Regurgitation and Arterial Hypertension. *Curr Vasc Pharmacol* 2019;**17**(2):180-190.

42. Losi MA, Izzo R, Mancusi C, Wang W, Roman MJ, Lee ET, Howard BV, Devereux RB, de Simone G. Depressed Myocardial Energetic Efficiency Increases Risk of Incident Heart Failure: The Strong Heart Study. *J Clin Med* 2019;**8**(7).

43. Siegel R, DeSantis C, Virgo K, Stein K, Mariotto A, Smith T, Cooper D, Gansler T, Lerro C, Fedewa S, Lin C, Leach C, Cannady RS, Cho H, Scoppa S, Hachey M, Kirch R, Jemal A, Ward E. Cancer treatment and survivorship statistics, 2012. *CA Cancer J Clin* 2012;**62**(4):220-41.

44. Plana JC, Galderisi M, Barac A, Ewer MS, Ky B, Scherrer-Crosbie M, Ganame J, Sebag IA, Agler DA, Badano LP, Banchs J, Cardinale D, Carver J, Cerqueira M, DeCara JM, Edvardsen T, Flamm SD, Force T, Griffin BP, Jerusalem G, Liu JE, Magalhaes A, Marwick T, Sanchez LY, Sicari R, Villarraga HR, Lancellotti P. Expert consensus for multimodality imaging evaluation of adult patients during and after cancer therapy: a report from the American Society of Echocardiography and the European Association of Cardiovascular Imaging. *Eur Heart J Cardiovasc Imaging* 2014;**15**(10):1063-93.

45. Herrmann J, Lerman A, Sandhu NP, Villarraga HR, Mulvagh SL, Kohli M. Evaluation and management of patients with heart disease and cancer: cardio-oncology. *Mayo Clin Proc* 2014;**89**(9):1287-306.

46. Zamorano JL, Lancellotti P, Rodriguez Munoz D, Aboyans V,

Asteggiano R, Galderisi M, Habib G, Lenihan DJ, Lip GYH, Lyon AR, Lopez Fernandez T, Mohty D, Piepoli MF, Tamargo J, Torbicki A, Suter TM, Group ESCSD. 2016 ESC Position Paper on cancer treatments and cardiovascular toxicity developed under the auspices of the ESC Committee for Practice Guidelines: The Task Force for cancer treatments and cardiovascular toxicity of the European Society of Cardiology (ESC). *Eur Heart J* 2016;**37**(36):2768-2801.

47. Charbonnel C, Convers-Domart R, Rigau deau S, Taksin AL, Baron N, Lambert J, Ghez S, Georges JL, Farhat H, Lambert J, Rousselot P, Livarek B. Assessment of global longitudinal strain at low-dose anthracycline-based chemotherapy, for the prediction of subsequent cardiotoxicity. *Eur Heart J Cardiovasc Imaging* 2017;**18**(4):392-401.

48. Desnick RJ, Brady R, Barranger J, Collins AJ, Germain DP, Goldman M, Grabowski G, Packman S, Wilcox WR. Fabry disease, an under-recognized multisystemic disorder: expert recommendations for diagnosis, management, and enzyme replacement therapy. *Ann Intern Med* 2003;**138**(4):338-46.

49. MacDermot KD, Holmes A, Miners AH. Anderson-Fabry disease: clinical manifestations and impact of disease in a cohort of 60 obligate carrier females. *J Med Genet* 2001;**38**(11):769-75.

50. MacDermot KD, Holmes A, Miners AH. Anderson-Fabry disease: clinical manifestations and impact of disease in a cohort of 98 hemizygous males. *J Med Genet* 2001;**38**(11):750-60.

51. D'Andrea A, Radmilovic J, Ballo P, Mele D, Agricola E, Cameli M, Rossi A, Esposito R, Novo G, Mondillo S, Montisci R, Gallina S, Bossone E, Galderisi M, Working Group on Echocardiography of the Italian Society of C. Left ventricular hypertrophy or storage disease? the incremental value of speckle tracking strain bull's-eye. *Echocardiography* 2017;**34**(5):746-759.

52. Phelan D, Collier P, Thavendiranathan P, Popovic ZB, Hanna M, Plana JC, Marwick TH, Thomas JD. Relative apical sparing of longitudinal strain using two-dimensional speckle-tracking echocardiography is both sensitive and specific for the diagnosis of cardiac amyloidosis. *Heart* 2012;**98**(19):1442-8.

53. Pica S, Sado DM, Maestrini V, Fontana M, White SK, Treibel T, Captur G, Anderson S, Piechnik SK, Robson MD, Lachmann RH, Murphy E, Mehta A, Hughes D, Kellman P, Elliott PM, Herrey AS, Moon JC. Reproducibility of native myocardial T1 mapping in the assessment of Fabry disease and its role in early detection of cardiac involvement by cardiovascular magnetic resonance. *J Cardiovasc Magn Reson* 2014;**16**:99.

54. Miyakis S, Lockshin MD, Atsumi T, Branch DW, Brey RL, Cervera R, Derksen RH, PG DEG, Koike T, Meroni PL, Reber G, Shoenfeld Y, Tincani A, Vlachoyiannopoulos PG, Krilis SA. International consensus statement on an

update of the classification criteria for definite antiphospholipid syndrome (APS). *J Thromb Haemost* 2006;**4**(2):295-306.

55. Nesher G, Ilany J, Rosenmann D, Abraham AS. Valvular dysfunction in antiphospholipid syndrome: prevalence, clinical features, and treatment. *Semin Arthritis Rheum* 1997;**27**(1):27-35.

56. Pardos-Gea J, Avegliano G, Evangelista A, Vilardell M, Ordi-Ros J. Cardiac manifestations other than valvulopathy in antiphospholipid syndrome: long-time echocardiography follow-up study. *Int J Rheum Dis* 2015;**18**(1):76-83.

57. Mikolasch TA, Garthwaite HS, Porter JC. Update in diagnosis and management of interstitial lung disease. *Clin Med (Lond)* 2016;**16**(Suppl 6):s71-s78.

58. Corra U, Piepoli MF, Adamopoulos S, Agostoni P, Coats AJ, Conraads V, Lambrinou E, Pieske B, Piotrowicz E, Schmid JP, Seferovic PM, Anker SD, Filippatos G, Ponikowski PP. Cardiopulmonary exercise testing in systolic heart failure in 2014: the evolving prognostic role: a position paper from the committee on exercise physiology and training of the heart failure association of the ESC. *Eur J Heart Fail* 2014;**16**(9):929-41.

59. Guazzi M, Arena R, Halle M, Piepoli MF, Myers J, Lavie CJ. 2016 Focused Update: Clinical Recommendations for Cardiopulmonary Exercise Testing Data Assessment in Specific Patient Populations. *Circulation* 2016;**133**(24):e694-711.

60. Messner-Pellenc P, Ximenes C, Brasileiro CF, Mercier J, Grolleau R, Prefaut CG. Cardiopulmonary exercise testing. Determinants of dyspnea due to cardiac or pulmonary limitation. *Chest* 1994;**106**(2):354-60.

61. Podolec P, Rubis P, Tomkiewicz-Pajak L, Kopec G, Tracz W. Usefulness of the evaluation of left ventricular diastolic function changes during stress echocardiography in predicting exercise capacity in patients with ischemic heart failure. *J Am Soc Echocardiogr* 2008;**21**(7):834-40.

62. van Riel AC, Opatowsky AR, Santos M, Rivero JM, Dhimitri A, Mulder BJ, Bouma BJ, Landzberg MJ, Waxman AB, Systrom DM, Shah AM. Accuracy of Echocardiography to Estimate Pulmonary Artery Pressures With Exercise: A Simultaneous Invasive-Noninvasive Comparison. *Circ Cardiovasc Imaging* 2017;**10**(4).

63. Myers J, Oliveira R, Dewey F, Arena R, Guazzi M, Chase P, Bensimhon D, Peberdy MA, Ashley E, West E, Cahalin LP, Forman DE. Validation of a cardiopulmonary exercise test score in heart failure. *Circ Heart Fail* 2013;**6**(2):211-8.

64. Nagueh SF, Smiseth OA, Appleton CP, Byrd BF, 3rd, Dokainish H, Edvardsen T, Flachskampf FA, Gillebert TC, Klein AL, Lancellotti P, Marino P, Oh JK, Popescu BA, Waggoner AD. Recommendations for the Evaluation of

Left Ventricular Diastolic Function by Echocardiography: An Update from the American Society of Echocardiography and the European Association of Cardiovascular Imaging. *J Am Soc Echocardiogr* 2016;**29**(4):277-314.

65. Nagueh SF, Appleton CP, Gillebert TC, Marino PN, Oh JK, Smiseth OA, Waggoner AD, Flachskampf FA, Pellikka PA, Evangelista A. Recommendations for the evaluation of left ventricular diastolic function by echocardiography. *J Am Soc Echocardiogr* 2009;**22**(2):107-33.

66. Cartlidge TR, Bing R, Kwiecinski J, Guzzetti E, Pawade TA, Doris MK, Adamson PD, Massera D, Lembo M, Peeters F, Couture C, Berman DS, Dey D, Slomka P, Pibarot P, Newby DE, Clavel MA, Dweck MR. Contrast-enhanced computed tomography assessment of aortic stenosis. *Heart* 2021.

67. Cui X, Li Y, Liu J, He S, Liu M. Aortic arch atheroma and the risk of stroke: a meta-analysis. *J Evid Based Med* 2014;**7**(3):185-91.

68. Rapsomaniki E, Timmis A, George J, Pujades-Rodriguez M, Shah AD, Denaxas S, White IR, Caulfield MJ, Deanfield JE, Smeeth L, Williams B, Hingorani A, Hemingway H. Blood pressure and incidence of twelve cardiovascular diseases: lifetime risks, healthy life-years lost, and age-specific associations in 1.25 million people. *Lancet* 2014;**383**(9932):1899-911.

69. Marwick TH, Gillebert TC, Aurigemma G, Chirinos J, Derumeaux G, Galderisi M, Gottdiener J, Haluska B, Ofili E, Segers P, Senior R, Tapp RJ, Zamorano JL. Recommendations on the use of echocardiography in adult hypertension: a report from the European Association of Cardiovascular Imaging (EACVI) and the American Society of Echocardiography (ASE) dagger. *Eur Heart J Cardiovasc Imaging* 2015;**16**(6):577-605.

70. Ho SY. Anatomy and myoarchitecture of the left ventricular wall in normal and in disease. *Eur J Echocardiogr* 2009;**10**(8):iii3-7.

71. de Simone G, Devereux RB. Rationale of echocardiographic assessment of left ventricular wall stress and midwall mechanics in hypertensive heart disease. *Eur J Echocardiogr* 2002;**3**(3):192-8.

72. Buckberg G, Mahajan A, Saleh S, Hoffman JI, Coghlan C. Structure and function relationships of the helical ventricular myocardial band. *J Thorac Cardiovasc Surg* 2008;**136**(3):578-89, 589 e1-11.

73. Sun JP, Lee AP, Wu C, Lam YY, Hung MJ, Chen L, Hu Z, Fang F, Yang XS, Merlino JD, Yu CM. Quantification of left ventricular regional myocardial function using two-dimensional speckle tracking echocardiography in healthy volunteers--a multi-center study. *Int J Cardiol* 2013;**167**(2):495-501.

74. Liu D, Hu K, Nordbeck P, Ertl G, Stork S, Weidemann F. Longitudinal strain bull's eye plot patterns in patients with cardiomyopathy and concentric left ventricular hypertrophy. *Eur J Med Res* 2016;**21**(1):21.

75. Rudolph A, Abdel-Aty H, Bohl S, Boye P, Zagrosek A, Dietz R, Schulz-Menger J. Noninvasive detection of fibrosis applying contrast-enhanced

cardiac magnetic resonance in different forms of left ventricular hypertrophy relation to remodeling. *J Am Coll Cardiol* 2009;**53**(3):284-91.

76. Mancusi C, Midtbo H, De Luca N, Halland H, de Simone G, Gerds E. Association of Myocardial Energetic Efficiency with Circumferential and Longitudinal Left Ventricular Myocardial Function in Subjects with Increased Body Mass Index (the FATCOR Study). *J Clin Med* 2021;**10**(8).

77. Santoro C, Arpino G, Esposito R, Lembo M, Paciolla I, Cardalesi C, de Simone G, Trimarco B, De Placido S, Galderisi M. 2D and 3D strain for detection of subclinical anthracycline cardiotoxicity in breast cancer patients: a balance with feasibility. *Eur Heart J Cardiovasc Imaging* 2017;**18**(8):930-936.

78. Minners J, Allgeier M, Gohlke-Baerwolf C, Kienzle RP, Neumann FJ, Jander N. Inconsistent grading of aortic valve stenosis by current guidelines: haemodynamic studies in patients with apparently normal left ventricular function. *Heart* 2010;**96**(18):1463-8.

79. Hinton RB, Jr., Lincoln J, Deutsch GH, Osinska H, Manning PB, Benson DW, Yutzey KE. Extracellular matrix remodeling and organization in developing and diseased aortic valves. *Circ Res* 2006;**98**(11):1431-8.

80. Yetkin E, Waltenberger J. Molecular and cellular mechanisms of aortic stenosis. *Int J Cardiol* 2009;**135**(1):4-13.

Curriculum Vitae

Surname and Name: Lembo Maria
Born: 22.06.1988 in Naples, Italy
Profession: Medical Doctor, Cardiologist
C F: LMBMRA88H62F839J
Contacts: +39 3405902890; maria.lembo@unina.it

Current Positions

May 2021 – present day Research Fellow at the Department of Advanced Biomedical Sciences, Federico II University of Naples, Italy.

Nov 2018 – present day International PhD programme in Cardiovascular Pathophysiology and Therapeutics (CardioPaTh), Federico II University of Naples, Italy.

Work experience

May 2021 – present day Research Fellow at the Department of Advanced Biomedical Sciences, Federico II University of Naples, Italy.

September 2021 – present day Clinical Cardiologist at the Hypertension Research Centre, Federico II University of Naples, Italy. (Director: Prof Raffaele Izzo).

Dec 2014 – Dec 2019 Clinical Fellow at the Laboratory of Standard and Advanced Echocardiography, Federico II University Hospital, Naples (Director: Prof Maurizio Galderisi).

May 2016 – Dec 2018 Clinical Fellow at the Coronary Care Unit, Federico II University Hospital, Naples (Director: Prof Bruno Trimarco).

Dec 2014 – Dec 2018	Clinical Fellow at the Cardiology Unit, Federico II University Hospital, Naples (Director Prof. Giovanni Esposito).
---------------------	---

Education and training

Jan 2020 – April 2021	Visiting fellow at the British Heart Foundation Centre of Cardiovascular Science, Cardiac imaging Unit, University of Edinburgh, UK. (Director: Prof David Newby).
-----------------------	--

Nov 2018 – present day	International PhD programme in Cardiovascular Pathophysiology and Therapeutics, Federico II University of Naples, Italy.
------------------------	--

Dec 2018	Residency in Cardiovascular Diseases with the maximal score of 50 (cum laude)/50 at the "Federico II" University of Naples, with an experimental thesis entitled: "Impact of the use of left ventricular mass/ end-diastolic volume ratio by 3D-echocardiography on 2D derived global longitudinal strain and diastolic function in native hypertensive patients". Supervisor Prof. Maurizio Galderisi.
----------	---

May 2018- Nov 2018	Clinical Fellow at Cardiovascular Department, Cardiac imaging Unit, Humanitas Clinical Institute IRCCS, Rozzano, Milan, Italy (Director: Prof Gianluigi Condorelli).
--------------------	--

Dec 2014 – Dec 2018	Residency in Cardiovascular Diseases at the "Federico II" University of Naples, Italy.
---------------------	--

Oct 2012 – Mar 2014	Resident student at the Department of Cardiovascular, Respiratory, Nephrological, Anesthesiological and Geriatric Sciences,
---------------------	---

Jul 2013

"Sapienza" University of Rome, Italy.

Degree in Medicine and Surgery with the maximal score of 110 (cum laude)/110 at

"Sapienza" University of Rome with an experimental thesis entitled: "Critical guidelines review for indication of ICD implantation in primary prevention in patients with heart failure: an integrated approach. Role of MIBG Scintigraphy and Cardiac Magnetic Resonance". Supervisor Prof. Francesco Fedele.

Awards

- 1) Best poster at the European Society of Cardiology Congress - The Digital Experience 2020 with the abstract: Lembo M, Santoro C, Casciano O, Capone V, Fedele T, Luciano F, Canonico ME, Buonauro A, Esposito R, Galderisi M. Impact of diastolic blood pressure on speckle tracking derived myocardial work components in a population of normotensive and untreated hypertensive patients.
- 2) Best poster at the European Society of Cardiology Congress, Munich 2018 with the abstract: Lembo M, Esposito R, Sorrentino R, Petitto M, Santoro C, Fazio V, Trimarco B, de Simone G, Galderisi M. Impact of the use of left ventricular mass/ end-diastolic volume ratio by 3D- echocardiography on 2D derived global longitudinal strain and diastolic function in native hypertensive patients.

Languages

Italian: native language

English: Optimal

Skills

Echocardiography: standard echo, Speckle tracking echocardiography, 3D-Echo, Physical and pharmacological (dobutamine and dipiridamole) stress echo, bubble test echo.

Cardiac Magnetic Resonance

Cardiac Computed Tomography

PET/CT cardiovascular imaging with 18F sodium fluoride

Computer Skills:

Windows Operating Systems Microsoft Office Package – Word, Excel, PowerPoint

Photo editing: Adobe Photoshop.

Elaboration and statistical analysis: GraphPad, SPSS.

Reviewer for the following journals:

E Clinical Medicine-The Lancet

Scientific Reports

Frontiers in Cardiovascular medicine

Memberships

Member of the Council of Hypertension of the European Society of Cardiology

Member of the Council of Cardio-oncology of the European Society of Cardiology

Member of the European Association of Cardiovascular Imaging

Member of the Italian Society of Cardiology

Publications

- 1) **Lembo M**, Manzi MV, Mancusi C, Morisco C, Rao MAE, Cuocolo A, Izzo R, Trimarco B. Advanced imaging tools for evaluating cardiac morphological and functional impairment in hypertensive disease. J Hypertens. 2021.

doi:10.1097/HJH.0000000000002967. Online ahead of print. Review

- 2) Cartlidge TR, Bing R, Kwiecinski J, Guzzetti E, Pawade TA, Doris MK, Adamson PD, Massera D, **Lembo M**, Peeters FECM, Couture C, Berman DS, Dey D, Slomka P, Pibarot P, Newby DE, Clavel MA, Dweck MR. Contrast-enhanced computed tomography assessment of aortic stenosis. *Heart*. 2021 Jan 29;heartjnl-2020-318556. doi: 10.1136/heartjnl-2020-318556.
- 3) Fletcher AJ, **Lembo M**, Kwiecinski J, Syed MJB, Nash J, Tzolos E, Bing R, Cadet S, MacNaught G, van Beek EJR, Moss AJ, Doris MK, Walker NL, Dey D, Adamson PD, Newby DE, Slomka PJ, Dweck MR. Quantifying microcalcification activity in the thoracic aorta. *J Nucl Cardiol*. 2021 Jan 20. doi: 10.1007/s12350-020-02458-w.
- 4) **Lembo M**, Santoro C, Sorrentino R, Fazio V, Canonico ME, Chiariello L, Galderisi M, Esposito R. Prominent basal and middle strain longitudinal involvement in newly-diagnosed and never treated hypertensive patients without clear-cut hypertrophy. *Int J Cardiol*. 2020 Apr 1;304:179-184. doi: 10.1016/j.ijcard.2020.01.038.
- 5) Buonauro A, Santoro C, Galderisi M, Canora A, Sorrentino R, Esposito R, **Lembo M**, Canonico ME, Ilardi F, Fazio V, Golia B, Sanduzzi A, Bocchino M. Impaired Right and Left Ventricular Longitudinal Function in Patients with Fibrotic Interstitial Lung Diseases. *J Clin Med*. 2020 Feb 21;9(2):587.

- 6) Cameli M and **Lembo M**, Sciaccaluga C, Bandera F, Ciccone MM, D'Andrea A, D'Ascenzi F, Esposito R, Evola V, Liga R, Mandoli GE, Palmiero P, Santoro C, Scicchitano P, Sorrentino R, Zito A, Pedrinelli R, Mondillo S, Mattioli AV, Galderisi M. Identification of cardiac organ damage in arterial hypertension: insights by echocardiography for a comprehensive assessment. *J Hypertens*. 2020 Apr;38(4):588-598. Review
- 7) Santoro C, Sorrentino R, Esposito R, **Lembo M**, Capone V, Rozza F, Romano M, Trimarco B, Galderisi M. Cardiopulmonary exercise testing and echocardiographic exam: an useful interaction. *Cardiovasc Ultrasound*. 2019 Dec 3;17(1):29. Review.
- 8) Santoro C, Galderisi M, Esposito R, Buonauro A, Monteagudo JM, Sorrentino R, **Lembo M**, Fernandez-Golfín C, Trimarco B, Zamorano JL. Global longitudinal strain is a hallmark of cardiac damage in mitral regurgitation: the Italian arm of the European Registry of mitral regurgitation (EuMiClip). *Cardiovasc Ultrasound*. 2019 Nov 21;17(1):28. doi: 10.1186/s12947-019-0178-7.
- 9) **Lembo M**, Santoro C, Sorrentino R, Canonico ME, Fazio V, Trimarco B, Tadic M, Galderisi M, Esposito R. Interrelation between midwall mechanics and Longitudinal strain in newly-diagnosed and never-treated hypertensive patients without clinically defined hypertrophy. *J Hypertens*. 2020 Feb;38(2):295-302.

- 10) Sorrentino R, Esposito R, Santoro C, Vaccaro A, Coccozza S, Scalamogna M, **Lembo M**, Luciano F, Santoro A, Trimarco B, Galderisi M. Practical impact of new diastolic recommendations on non-invasive estimation of left ventricular diastolic function and filling pressures. *J Am Soc Echocardiogr* 2019 Oct 13. pii: S0894-7317(19)30924-1. doi: 10.1016/j.echo.2019.08.013.
- 11) Santoro C, Esposito R, **Lembo M**, Sorrentino R, De Santo I, Luciano F, Casciano O, Giuliano M, De Placido S, Trimarco B, Lancellotti P, Arpino G, Galderisi M. Strain-oriented strategy for guiding cardioprotection initiation of breast cancer patients experiencing cardiac dysfunction. *Eur Heart J Cardiovasc Imaging*. 2019 Dec 1;20(12):1345-1352.
- 12) Tufano A, Di Minno MND, Guida A, **Lembo M**, Di Minno G, Galderisi M. Cardiac Manifestations of Antiphospholipid Syndrome: Clinical Presentation, Role of Cardiac Imaging, and Treatment Strategies. *Semin Thromb Hemost*. 2019 Jul;45(5):468-477.
- 13) **Lembo M**, Santoro C, Sorrentino R, Trimarco B, Galderisi M, Esposito R. Impact of left ventricular mass/end-diastolic volume ratio by three-dimensional echocardiography on two-dimensional global longitudinal strain and diastolic function in native hypertensive patients. *J Hypertens*. 2019 Oct;37(10):2041-2047.
- 14) Esposito R, Galderisi M, Santoro C, Imbriaco M, Riccio E, Pellegrino AM, Sorrentino R, **Lembo M**, Citro R, Losi MA,

Spinelli L, Trimarco B, Pisani A. Prominent longitudinal strain reduction of left ventricular basal segments in treatment-naïve Anderson-Fabry disease patients.

Eur Heart J Cardiovasc Imaging. 2019 Apr 1;20(4):438-445.

- 15) Petitto M, Esposito R, Sorrentino R, **Lembo M**, Luciano F, De Roberto AM, La Mura L, Pezzullo E, Maffei S, Galderisi M, Lancellotti P. Gender specific echocardiographic reference values: the female's point of view. Journal of Cardiovascular Medicine 2018;19:527-535.
- 16) Tufano A, **Lembo M**, Di Minno MND, Nardo A, Esposito R, Santoro C, Buonauro A, Cerbone AM, Di Minno G, Galderisi M. Left ventricular diastolic abnormalities other than valvular heart disease in Antiphospholipid Syndrome: an echocardiographic study. Int J Cardiol. 2018;271:366-370.
- 17) Cadeddu Dessalvi C, Deidda M, Mele D, Bassareo PP, Esposito R, Santoro C, **Lembo M**, Galderisi M, Mercurio G. Chemotherapy-induced cardiotoxicity: new insights into mechanisms, monitoring, and prevention. J Cardiovasc Med (Hagerstown). 2018 Jul;19(7):315-323.
- 18) **Lembo M**, Esposito R, Santoro C, Lo Iudice F, Schiano-Lomoriello V, Fazio V, Grimaldi MG, Trimarco B, de Simone G, Galderisi M. Three dimensional echocardiographic ventricular mass/end-diastolic volume ratio in native hypertensive patients: relation between stroke volume and geometry. J Hypertens. 2018 Aug;36(8):1697-1704.
- 19) Alcidi GM, Esposito R, Evola V, Santoro C, **Lembo M**, Sorrentino R, Lo Iudice F, Borgia F, Novo G, Trimarco B,

Lancellotti P, Galderisi M. Normal reference values of multilayer longitudinal strain according to age decades in a healthy population: A single-centre experience. *Eur Heart J Cardiovasc Imaging*. 2018 Dec 1;19(12):1390-1396.

- 20) **Lembo M**, Sicari R, Esposito R, Rigo F, Cortigiani L, Lo Iudice F, Picano E, Trimarco B, Galderisi M.
Association Between Elevated Pulse Pressure and High Resting Coronary Blood Flow Velocity in Patients With Angiographically Normal Epicardial Coronary Arteries. *J Am Heart Assoc*. 2017 Jun 29;6(7). pii: e005710.
- 21) Buonauro A, Galderisi M, Santoro C, Canora A, Bocchino ML, Lo Iudice F, **Lembo M**, Esposito R, Castaldo S, Trimarco B, Sanduzzi A. Obstructive sleep apnoea and right ventricular function: A combined assessment by speckle tracking and three-dimensional echocardiography. *Int J Cardiol*. 2017 Sep 15;243:544-549
- 22) Santoro C, Arpino G, Esposito R, **Lembo M**, Paciolla I, Cardalesi C, de Simone G, Trimarco B, De Placido S, Galderisi M. 2D and 3D strain for detection of subclinical anthracycline cardiotoxicity in breast cancer patients: a balance with feasibility. *Eur Heart J Cardiovasc Imaging*. 2017 May 1;18:930-936.
- 23) **Lembo M**, Esposito R, Lo Iudice F, Santoro C, Izzo R, De Luca N, Trimarco B, de Simone G, Galderisi M.
Impact of pulse pressure on left ventricular global longitudinal strain in normotensive and newly diagnosed, untreated hypertensive patients. *J Hypertens*. 2016

Jun;34(6):1201-1207.

- 24) Carrizzo A, Forte M, **Lembo M**, Formisano L, Puca AA, Vecchione C. Rac-1 as a new therapeutic target in cerebro- and cardio-vascular diseases. *Curr Drug Targets*. 2014;15(13):1231-1246.
- 25) Kisialiou A, Grella R, Carrizzo A, Pelone G, Bartolo M, Zucchella C, Rozza F, Grillea G, Colonnese C, Formisano L, **Lembo M**, Puca AA, Vecchione C. Risk factors and acute ischemic stroke subtypes. *J Neurol Sci*. 2014 Apr 15;339(1-2):41-6.

Conference proceedings

- 1) **Lembo M**, Santoro C, Casciano O, Capone V, Fedele T, Luciano F, Canonico ME, Buonauro A, Esposito R, Galderisi M.
Impact of diastolic blood pressure on speckle tracking derived myocardial work components in a population of normotensive and untreated hypertensive patients.
ESC Congress - The Digital Experience 29 August- 1 September 2020 (*evaluated as one of the best posters*)
- 2) **Lembo M**, Esposito R, Santoro C, Sorrentino R, Luciano F, Casciano O, Fiorillo L, La Mura L, Canonico ME, Galderisi M.
Prominent longitudinal strain involvement of left ventricular basal segments in native hypertensive patients without clear-cut hypertrophy.
Euroecho Wien 4-7 December 2019, oral communication

- 3) **Lembo M**, Fazio V, Capone V, Esposito L, Sorrentino R, Santoro C, Esposito R, Galderisi M.
Impact of hyperuricemia on left ventricular longitudinal systolic function in uncomplicated hypertensive patients.
Euroecho Wien 4-7 December 2019
- 4) **Lembo M**, Sorrentino R, Santoro C, Esposito R, Scalamogna M, Avvedimento M, Magliulo F, Franzone A, Cirillo P, Esposito G, Galderisi M.
Impact of transcatheter aortic valve implantation on concomitant mitral regurgitation in patients with severe aortic stenosis.
Euroecho Wien 4-7 December 2019.
- 5) **Lembo M**, Esposito R, Santoro C, Sorrentino R, Sellitto V, Luciano F, Casciano O, Scalamogna M, Trimarco B, Galderisi M.
Prominent longitudinal strain involvement of left ventricular base in native hypertensive patients without clear-cut hypertrophy.
79th National Congress of the Italian Society of Cardiology, Rome 14-17 December 2018, oral communication.
- 6) **Lembo M**, Esposito R, Santoro C, Fazio V, De Roberto AM, Mancusi C, Trimarco B, de Simone G, Galderisi M.
Independent association between left ventricular midwall mechanics and global longitudinal strain in native hypertensive patients.
XXXV National congress of Italian society of arterial

hypertension, Rome 27-29 September 2018, oral communication.

- 7) **Lembo M**, Esposito R, Sorrentino R, Petitto M, Santoro C, Fazio V, Trimarco B, de Simone G, Galderisi M.
Impact of the use of left ventricular mass/ end-diastolic volume ratio by 3D- echocardiography on 2D derived global longitudinal strain and diastolic function in native hypertensive patients.
XXXV National congress of Italian society of arterial hypertension, Rome 27-29 September 2018.
- 8) **Lembo M**, Esposito R, Sorrentino R, Petitto M, Santoro C, Fazio V, Trimarco B, de Simone G, Galderisi M.
Impact of the use of left ventricular mass/ end-diastolic volume ratio by 3D- echocardiography on 2D derived global longitudinal strain and diastolic function in native hypertensive patients.
ESC Congress Munich 25-29 August 2018 (*evaluated as one of the best posters*).
- 9) **Lembo M**, Esposito R, Santoro C, Fazio V, De Roberto AM, Mancusi C, Trimarco B, de Simone G, Galderisi M.
Independent association between left ventricular midwall mechanics and global longitudinal strain in native hypertensive patients.
ESC Congress Munich 25-29 August 2018.
- 10) **Lembo M**, Petitto M, Esposito R, Fazio V, Santoro C, Lo Iudice F, De Roberto AM, Trimarco B, Galderisi M.
Ventricular interdependence in the hypertensive heart: the

use of speckle tracking echocardiography
78th National Congress of the Italian Society of Cardiology,
Rome 15-18 December 2017, oral communication.

- 11) **Lembo M**, Petitto M, Esposito R, Fazio V, Santoro C, Lo Iudice F, De Roberto AM, Trimarco B, Galderisi M.
Ventricular interdependence in the hypertensive heart: insights by speckle tracking echocardiography.
Euroecho Lisbon 6-9 December 2017
- 12) **Lembo M**, Alcidi GM, Santoro C, Esposito R, Esposito L, De Roberto AM, Galderisi M.
Atrial fibrillation during adjuvant therapy of breast cancer: the role of Global Longitudinal Strain for an appropriate diagnosis of cardiotoxicity.
Euroecho Lisbon 6-9 December 2017
- 13) **Lembo M**, Petitto M, Esposito R, Santoro C, Lo Iudice F, Avvedimento M, Fazio V, de Simone G, Trimarco B, Galderisi M.
Ventricular interdependence in the hypertensive heart: the use of Speckle tracking echocardiography.
XXXIV National congress of Italian society of arterial hypertension, Milano 5-7 October 2017, oral communication
- 14) **Lembo M**, Lo Iudice F, Esposito R, Santoro C, Gerardi D, Trimarco B, de Simone G, Galderisi M.
Left ventricular mass/end-diastolic volume ratio using tridimensional echocardiography in newly-diagnosed hypertensive patients: relation between left ventricular

geometry and stroke volume.

77th National Congress of the Italian Society of Cardiology,
Rome 16-19 December 2016, oral communication

- 15) **Lembo M**, Tufano A, Nardo A, Buonauro A, Fazio V, Schiano Lomoriello V, Santoro C, Cocozza S, Di Minno G, Trimarco B, Galderisi M.

2D Echocardiographic left ventricular diastolic abnormalities other than valvular disease in Antiphospholipid Syndrome.
77th National Congress of the Italian Society of Cardiology,
Rome 16-19 December 2016, oral communication

- 16) **Lembo M**, Santoro C, Esposito R, Gerardi D, Sellitto V, Trimarco B, Galderisi M.

The detection of early left ventricular dysfunction by Global Longitudinal Strain is helpful to keep in adjuvant therapy breast cancer patients till completion
Euroecho Leipzig 7-10 December 2016

- 17) **Lembo M**, Lo Iudice F, Esposito R, Santoro C, Gerardi D, Trimarco B, de Simone G, Galderisi M.

Left ventricular mass/end-diastolic volume ratio with tridimensional echocardiography in newly-diagnosed hypertensive patients: what relation between left ventricular geometry and stroke volume?
Euroecho Leipzig 7-10 December 2016

- 18) **Lembo M**, Tufano A, Nardo A, Buonauro A, Fazio V, Schiano Lomoriello V, Santoro C, Cocozza S, Di Minno G, Trimarco B, Galderisi M.

Left ventricular abnormalities other than valvular disease in

antiphospholipid syndrome: an echocardiographic study.

Euroecho Leipzig 7-10 December 2016, oral communication

- 19) **Lembo M**, Rigo F, Cortigiani L, Gherardi S, Sicari R, Picano E, Trimarco B, Galderisi M.

Independent association between pulse pressure and resting coronary flow velocity in hypertensive patients with angiographically normal coronary arteries.

XXXIII National congress of Italian society of arterial hypertension, Firenze 6-8 October 2016, oral communication.

- 20) **Lembo M**, Lo Iudice F, Esposito R, Santoro C, Gerardi D, Trimarco B, de Simone G, Galderisi M.

Left ventricle mass / volume ratio with three-dimensional echocardiography in newly diagnosed hypertension: what relationship between ventricular geometry and stroke volume?

XXXIII National congress of Italian society of arterial hypertension, Firenze 6-8 October 2016

- 21) **Lembo M**, Lo Iudice F, Esposito R, Santoro C, Izzo R, de Simone G, Trimarco B, Galderisi M.

Impact of pulse pressure on global longitudinal strain in a population of normotensive and newly diagnosed never treated hypertensive subjects

76th National Congress of the Italian Society of Cardiology, Rome 11-14 December 2015, oral communication.

- 22) **Lembo M**, Lo Iudice F, Esposito R, Santoro C, Coccozza S, Izzo R, De Luca N, de Simone G, Trimarco B, Galderisi M.

Independent association between pulse pressure and left ventricular global longitudinal strain.

Euroecho Seville 2-5 December 2015

- 23) **Lembo M**, Lo Iudice F, Esposito R, Santoro C, Izzo R, De Luca N, de Simone G, Trimarco B, Galderisi M.

Impact of the pulse pressure on left ventricular global longitudinal strain in patients with uncomplicated arterial hypertension

XXXII National congress of Italian society of arterial hypertension, Bologna 24-26 September 2015

- 24) **Lembo M**, Bruno N, Salvi N, Adamo F, Foschi ML, Mancone M, Brasolin B, De Vincentis G, Fedele F.

Role of 123-iodine metaiodobenzylguanidine imaging in identifying heart failure patients at high risk for sudden cardiac death: a real world single centre experience.

74th National Congress of the Italian Society of Cardiology, Rome 14-16 December 2013, oral communication.

By invitation

- 1) Multimodality imaging approach to Fabry cardiomyopathy. The role of speckle tracking echocardiography for an early diagnosis.

Euroecho Wien 4-7 December 2019, speaker

- 2) 3D Speckle tracking echocardiography

Course of cardiac and thoracic echo “Cuore e... dintorni”,

Naples 29-30 October 2019, speaker and tutor

- 3) The role of strain imaging in cardiotoxicity subclinical diagnosis
Theoretical-practical course on cardio-onco-haematology: from diagnosis to management, Naples 26-27 September 2019, speaker and tutor
- 4) The role of advanced cardiac imaging for diagnosis and management of myocarditis
XI Arca Imaging congress, Matera 13-14 September 2019, speaker
- 5) A new method to approach stress-echo: from strain to 3D imaging with high frame rate
XVI National congress of coronary and cardiac multi-imaging, Naples 19-20 March 2019, speaker, tutor and scientific secretary member
- 6) Medact: update workshop for young medical doctors
Naples 19-20 October 2018, speaker
- 7) Angiographic scores and strain rate imaging: the additional value of echocardiographic quantitative technology
XVI National congress of coronary and cardiac multi-imaging, Naples 12-13 April 2018, speaker, tutor and scientific secretary member.
- 8) Tissue Doppler and Speckle tracking echocardiography at patients' bedside;
Primary and secondary mitral valve regurgitation
Echocardiographic course: intermediate level theoretical-practical course, Naples 27-29 November 2017, speaker and

tutor.

- 9) The role of registries in real life: the COT registry of the European society of Cardiology in breast cancer patients
IX Arca Imaging congress, Naples 15-16 September 2017, speaker.
- 10) A clinical case of subclinical cardiotoxicity successfully managed following ASE/EACVI recommendations.
XV National congress of coronary and cardiac multi-imaging, Naples 19-20 May 2017, speaker and tutor.

Acknowledgments

This PhD path has represented a big source of training and experience in both research and clinic, thanks to all the people who supported me during this journey.

I would like to sincerely thank Prof. Bruno Trimarco for his everlasting guidance and for his foresight in suggesting me to approach cardiac imaging, introducing me to Prof. Maurizio Galderisi.

I would never thank enough Maurizio for giving me the opportunity to discover advanced imaging techniques and for passing down to me the passion for this topic. He taught me the art of echocardiography and how to write a scientific paper. His departure in the middle of my PhD was a great shock, but I will always keep his words and teachings in my mind and heart.

I wish to profoundly thank Prof. Raffaele Izzo for his valuable support, encouragement, and constructive advice.

I am extremely grateful to Prof. David Newby for welcoming me to the British Heart Foundation Centre of Cardiovascular Science at the University of Edinburgh and for giving me the opportunity to attend his department. My deepest thanks to Prof. Marc Dweck for his support and ingenious ideas, which opened my mind to new approaches and possibilities in advanced cardiac imaging. A big thanks to all the people of the Edinburgh team for their patience and expertise, and for guiding me in my foreign experience.

A sincere thanks to Prof. Emanuele Barbato for his tireless guidance as coordinator of the CardioPaTh PhD program.

Finally, a deep thanks to my family, my pillar in life, first supporter and provider of wise counsel.